Radiative capture of π^- mesons and spin–isospin excitations of nuclei

M. Gmitro

Joint Institute for Nuclear Research and Institute of Nuclear Physics, Czechoslovak Academy of Sciences, Řež

H. R. Kissener

Central Institute of Nuclear Research, Rossendorf

P. Truöl

Physics Institute, Zurich University

R. A. Éramzhyan

Institute of Nuclear Research, USSR Academy of Sciences, Moscow

Fiz. Elem. Chastits At. Yadra **14**, 773–834 (July–August 1983)

The radiative capture of stopped pions by light nuclei is analyzed in detail. It is shown that the structure of the excitation spectrum of $1p$-shell nuclei is due to concentration of the strengths of the transitions that in the initial nucleus form the $M1$ and $M2$ resonances. Radiative capture in heavier nuclei, in which a resonance structure is hardly manifested, is also considered. One of the sections of the review is devoted to the phenomenological approach in the description of the radiative capture of pions. In the final part there is a brief discussion of the related process of radiative in-flight capture of pions. The review ends with a discussion of the prospects for further development of investigations in this field of nuclear physics.

PACS numbers: 25.80.Hp, 27.20. + n

INTRODUCTION

In our review of Ref. 1 on radiative capture of pions by nuclei, we considered essentially only two questions: radiative capture by few-nucleon systems and by the ^{16}O nucleus. The main mechanisms of radiative capture of pions by nuclei were discussed for the example of ^{16}O, and the possibilities of using this reaction as a new tool in the investigation of nuclear structure were demonstrated. Detailed analysis of the response of the nucleus in the $^{16}O(\pi,\gamma)$ reaction also made it possible to demonstrate the possibilities of fairly complicated theoretical models proposed for the description of the structure of nuclear states.[1)] The fact that for ^{16}O there exists an extensive set of diverse experimental data was a further, and not the least important reason for the choice of a specific nucleus. The availability of such information made it possible to compare the radiative capture of pions with reactions induced by other particles and to establish general features of the nuclear response independent of the details of nuclear structure. The discussion of this material was already sufficient to show that in the time that had elapsed since the publication of the two extensive reviews of Refs. 2 and 3 on the problem of the (π,γ) reaction significant progress had been achieved in this field of intermediate-energy physics.

An important conclusion drawn in Ref. 1 was that a satisfactory description of the (π,γ) reaction on ^{16}O has been achieved. A good basis is therefore available for interpreting the nuclear response in this process, not only in nuclei neighboring ^{16}O but also in nuclei fairly far from it. Of course, one cannot yet give as complete a treatment as for ^{16}O, for which many factors important for the description of nuclear structure have been taken into account. Therefore, the extended theory is primarily semiquantitative in nature and aims in the first place at establishing the basic features of the excitation of nuclei in the (π,γ) reaction.

As we have already noted in Ref. 1, the nature of the elementary excitation is such that spin excitations of the nucleus are decisive. In light nuclei, these are spin-monopole (magnetic dipole) and spin-dipole (magnetic quadrupole and transverse $E1$) excitations. Discussion of this question occupies a central position in the review. So far, radiative capture of pions has been investigated in detail only in nuclei of the $1p$ shell—from lithium to oxygen. The theory is capable of describing a large set of experimental data. It is in these nuclei that the resonance structure of the excitation spectrum is most clearly revealed.

In this review, we analyze in detail the situation in nuclei of the $1p$ shell. We also consider a number of examples of radiative capture of pions in nuclei of the $(2s-1d)$ shell, in which structure is also observed in the hardest part of the γ spectrum. We conclude with two examples of radiative capture of pions by the heavy nuclei ^{208}Pb and ^{209}Bi. The following section of the review is devoted to the phenomenological approach in the description of radiative capture of pions. We consider

[1)] In Ref. 1, there are errors in Table XIX. We give the table here in its corrected form:

Model	Λ_{1s}, 10^{16}sec^{-1}	Λ_{2p}, 10^{12} sec^{-1}	R_a, 10^{-4}	R_b, 10^{-4}	Reference
TDAC	32.5	219.3	126	305	[106]
EGSA	39.0	167.9	101	244	[103]
ESMA	23.4	148.6	86	208	[103]

$R_a = (0.3047 \cdot 10^{-16}\ \Lambda_{1s} + 0.5239 \cdot 10^{-12}\ \Lambda_{2p}) \cdot 10^{-4}$
$R_b = (0.7400 \cdot 10^{-16}\ \Lambda_{1s} + 1.2814 \cdot 10^{-12}\ \Lambda_{2p}) \cdot 10^{-4}$

 0090-4759/83/040323-26$04.40 © 1984 American Institute of Physics

some examples of partial transitions in such capture, whose characteristics can be related to those of other transitions (electromagnetic and weak) almost without the use of model wave functions. In the last part of the review we discuss the radiative capture of pions in flight. The review ends with a discussion of the prospects for further development of investigations in this field of nuclear physics.

1. RESPONSE OF A 1p NUCLEUS TO RADIATIVE CAPTURE OF A PION

General considerations

In the review of Ref. 1, we analyzed in detail the structure of the transition operator in the radiative capture of pions and established that in light nuclei the following multipole components of the operators play the decisive part:

$$\hat{O}_{112} \sim [\sigma \otimes Y_1]_2; \tag{1a}$$

$$\hat{O}_{111} \sim [\sigma \otimes Y_1]_1. \tag{1b}$$

In electron scattering, the operator (1a) is responsible for magnetic quadrupole excitations ($M2$), and the operator (1b) is manifested in transverse electric dipole ($E1t$) excitations. Besides (1a) and (1b), an appreciable part in radiative capture of pions is played by the spin–quadrupole components

$$\hat{O}_{12J} \sim [\sigma \otimes Y_2]_J, \tag{1c}$$

especially if capture takes place from the $2p$ orbit of the mesic atom. These transitions are localized in the region of high excitations of the nucleus. In addition to those already listed, the spin-monopole component of the operator of the (π,γ) transition,

$$\hat{O}_{101} \sim [\sigma \otimes Y_0]_1, \tag{1d}$$

must also be manifested; it is the analog of the spin part of the operator of the isovector $M1$ transition in electron scattering.

The shell model is widely used to describe the response of a nucleus to an external field. In Ref. 4 a many-particle variant of the shell model was developed for $1p$ nuclei, the construction of the wave functions taking into account all admissible configurations in the band of $0\hbar\omega$ and $1\hbar\omega$ nucleon excitation. This is an important step in describing the nuclear response, since then the energy spread of the transition strengths can be correctly reproduced. Such an approach was first used[5] to describe photonuclear resonance in the $1p$ nuclei ^{7}Li, ^{9}Be, ^{13}C, ^{14}C, ^{14}N, and ^{15}N. Not only the total but also the partial excitation spectra, when the state of the final A-1 nucleus formed after emission of the nucleon is fixed, were calculated. Comparison with numerous experimental data showed that overall the theory correctly reproduces the structure of the total and partial spectra. However, this approach still does not give a quantitatively rigorous description of the processes, the theory overestimating the concentration of the transition strengths in the region of the maximum of the resonance.

Wave functions of 1p-shell nuclei in the framework of the many-particle shell model

We consider briefly the main aspects of the construction of the wave functions of the $1p$-shell nuclei in the framework of the shell model. We proceed from Ref. 4, which uses a unified set of parameters for all this region of nuclei. For some transitions, particularly for ^{10}B and ^{12}C, we shall give results obtained by other authors with a different parameter set[6-8]—for technical reasons, the wave functions of the last two nuclei could not be constructed in Ref. 4.

The single-particle wave functions are usually calculated in the harmonic-oscillator potential. The spurious states corresponding to the excitation of the center of mass of the nucleus are rigorously eliminated in Ref. 4. The nuclear Hamiltonian includes the interaction between the nucleons in the $1p$ shell and between nucleons in different shells, for example, $\langle 1p1d|V|1p1d\rangle$, and also the set ε_{nlj} of single-particle energies. The interaction between the $1p$ nucleons is described by the set of matrix elements (8–16) $2BME$ proposed by Cohen and Kurath (CK).[9] The interaction of nucleons in different shells is described by the modified variant of the Gillet potential[11] proposed in Ref. 10; in what follows, we shall denote this potential by COP. The modification is obtained by slightly correcting the interaction parameters used in Ref. 11 in order to reproduce better the positions of the low-lying levels corresponding to $1\hbar\omega$ excitations.[10] A detailed optimization of the parameter set was not made. The primary aim of such a calculation is not a highly accurate quantitative description of the various characteristics of the processes in each particular nucleus but is rather to bring out the tendencies in the complete region of investigated nuclei. The functions obtained in this way were used to calculate the rates of electromagnetic transitions, muon capture, and radiative pion capture. Comparison with the experimental data showed that such an approach is already capable of successfully reflecting many observed features. In what follows, we shall call the variant of the calculation based on the CK+ COP interaction the *standard* variant.

To investigate the stability of the result with respect to variation of the parameters, calculations were made with a different variant of the interaction. This variant, which we shall denote by MK, was proposed in Ref. 12 to improve the agreement between theory and experiment in the positions of the levels corresponding to $1\hbar\omega$ excitations of the ^{11}B nucleus. In contrast to the COP interaction, the MK interaction also contains a contribution of noncentral forces. The matrix elements of the two-body interaction calculated in the MK variant are close to the matrix elements obtained from the G matrix corresponding to the Hamada–Johnston potential.[13] The CK+ MK potential leads to somewhat better agreement with experiment (see Ref. 10) for the positions of the low-lying levels corresponding to $1\hbar\omega$ excitation than the CK+ COP potential. With regard to the gross structure of the dipole resonance, except for the nuclei with A= 7 and 11 appreciable differences are not observed.

In the nuclei with $A = 6$, the low-lying states are not very well described by the wave functions obtained using the CK Hamiltonian. Therefore, in this case the states corresponding to $0\hbar\omega$ excitations were described by means of the wave functions of Ref. 14. The wave functions of the states corresponding to $1\hbar\omega$ excitations were calculated using the Rosenfeld interaction,[15] the position of the levels being fixed by the peak of quasielastic knockout of 1s protons from the ^{7}Li nucleus: $^7\text{Li}(p, 2p)^6\text{He}$.

The result of the analysis of the various reactions—photonuclear, electron scattering, μ capture, radiative pion capture—in the framework of the standard approach can be formulated as follows: When agreement is obtained between theory and experiment in the description of the (π, γ) reaction, it is also achieved for the photodisintegration reactions and electron scattering. The positions of the main maxima are reproduced by the theory fairly well in all reactions, and their deviations from the experimental positions do not exceed 1–2 MeV. In the ^{7}Li and ^{11}B nuclei both the (π, γ) reaction and the photodisintegration are poorly described in the framework of the standard set of parameters. The main peaks in the nuclear excitation spectrum are appreciably shifted to lower excitation energies. If the MK interaction is used, the agreement between theory and experiment is much better. We shall continue the discussion of this question below.

It follows from what has been said above that we shall discuss radiative capture of pions by $1p$ nuclei mainly in the framework of the shell model, which does not take into account directly continuum states. The relationship between these two approaches and the part played by the continuum[7,16] were discussed in detail in Ref. 1 for the example of ^{16}O. Here, we give the results of the calculation of Ref. 7 with allowance for the continuum for the ^{12}C nucleus.

To make possible direct comparison with experiment of the results of calculation in the framework of the model without allowance for the continuum, it was assumed that each resonance has a Breit–Wigner shape. All resonances were assumed to have the same width. Another possibility is to use calculated values of the widths.

Total and partial transition rates

Using the wave functions discussed above and the impulse approximation with the effective Hamiltonian

$$H_{\text{eff}} = \sum_{j=1}^{A} \exp(-i\mathbf{k}\cdot\mathbf{x}_j) \int d^3r \delta(\mathbf{r}-\mathbf{x}_j) H_j \Phi_{nlm}(\mathbf{r}) \tau_j^-,$$

we can calculate the rates Λ_{nl} of capture from the nl orbit of the mesic atom. To calculate the experimentally measured yield of γ rays,

$$R = \omega_s \Lambda_{1s}/\Gamma_{1s}^{abs} + \omega_p \Lambda_{2p}/\Gamma_{2p}^{abs} + \ldots,$$

we must have recourse to the experimental values of the mesoatomic characteristics ω_l and Γ_{nl}^{abs}. In Ref. 1 we have given (in Table VI) their numerical values, and also the expressions needed to calculate the partial rates Λ_{nl} (see Eq. (28) and the following equations in Ref. 1). Summation of all the partial transitions gives the total rate of the (π, γ) reaction and the total γ yield. The calculated and measured total γ yields for $1p$ nuclei are given in Table I.

Before we compare the calculated and measured total yields, we note some general features that can be traced on the transition from light to heavy nuclei. The γ yield from radiative capture of pions does not change strongly with increasing charge Z of the nucleus even when, for example, μ capture reveals a strong dependence of the total capture rate Λ_μ on the number of protons. The reason for this is that the γ yield is a relative quantity; it is divided by the total rate of absorp-

TABLE I. Experimental values of the total rate of μ^- capture, the γ yields in radiative pion capture by nuclei of the $1p$ shell, and theoretical values of the yields R_s, R_p, and R_γ calculated in the standard (see the text) version and with the MK interaction.[8]

Nucleus	J_i	Λ_μ, 10^4 sec^{-1}	R_γ^π, 10^{-3}		R_s, 10^{-3}		R_p, 10^{-3}		N_0[c]	N_1[c]	Γ_{1s}^π, eV	$\frac{R_\gamma^\pi \Gamma_{1s}^\pi}{\hbar\Lambda_\mu}$, 10^{12}
		experiment	experiment[a]	theory	$0\hbar\omega$	$1\hbar\omega$	$0\hbar\omega$	$1\hbar\omega$				
^{6}Li	1^+	0.468±0.012 [20]	42.2±2.5	32.4	4.3	15.2	3.0	9.9	5	47	195±12	2.67±0.24
^{7}Li	$3/2^-$	0.226±0.012 [20]	18.2±0.9	20.9	0.47	10.4	0.61	9.4	5	74	195±13	2.39±0.24
^{7}Li[b]				20.5	0.47	10.1	0.61	9.3				
^{9}Be	$3/2^-$	1.00±0.21	24.8±2.8	12.9	0.51	6.3	0.39	5.7	19	294	591±14	2.23±0.53
^{10}B	3^+	2.58±0.15	23.5±0.9								1680±120	2.33±0.23
^{11}B	$3/2^-$	2.12±0.15	17.7±1.0	17.2	0.49	3.2	1.1	12.4	19	455	1720±150	2.18±0.27
^{11}B[b]				17.1	0.49	3.2	1.1	12.3				
^{12}C	0^+	3.71±0.11	17.7±0.6								3120±210	2.26±0.18
^{13}C	$1/2^-$	—	16.6±0.5	16.6	0.39	2.6	0.95	12.7	5	241	2590±110	—
^{14}C	0^+	—	6.5±1.8	15.0	—	2.0	—	13.0	—	47		—
^{14}N	1^+	6.44±0.35	20.0±0.8	20.9	0.59	2.8	2.1	15.4	5	191	4480±300	2.11±0.20
^{15}N	$1/2^-$	—	—	17.7	—	2.7	—	15.0	—	36		—
^{16}O	0^+	97.4±3.1	22.7±2.4	20.8[e]	—	1.4	—	10.3	—	12	7560±500	2.67±0.32
^{18}O	0^+	—	19.6±2.2									

[a] A complete list of experimental results and references can be found in Table VII in the review of Ref. 1.
[b] The interaction from Ref. 12 was used in the calculation.
[c] The number N_n is the number of states of the final nucleus in the band $n\hbar\omega$.
[d] Mean value: $(2.23 \pm 0.09) \times 10^{12}$ ($\chi^2 = 4.9$).
[e] Nuclear excitations in the $2\hbar\omega$ excitation band are included.
References to the remaining results of measurements of the μ-capture rate can be found in Refs. 3 and 21.

tion of pions. Such a characteristic depends weakly on the charge of the nucleus and on the number of nucleons. The growth of the total rate of μ capture with increasing Z reflects the stronger overlapping of the muon and nuclear functions.

We multiply the γ yield R by the total width of the 1s level of the pionic atom, which reflects the degree of overlapping of the pion and nuclear functions:

$$R\Gamma_{1s} = \omega_s(Z)\,\Lambda_{1s}(Z) + \omega_p(Z)\,\frac{\Gamma_{1s}(Z)}{\Gamma_{2p}(Z)}\,\Lambda_{2p}(Z). \qquad (2)$$

The number then obtained (see Table I) can be taken as a rough estimate of the observed radiative capture rate. This characteristic behaves in the same way as the total rate of μ capture. In particular, in both reactions we observe a strong isotopic effect in the Li isotopes and a somewhat weaker effect in the B isotopes (see Table I). It follows from this in particular that the states of the final nucleus populated as a result of absorption of a muon by a bound proton and radiative pion capture are basically the same. The decrease in the reaction rate with increasing number of neutrons is caused by the blocking effect due to the Pauli principle and is associated with the presence of an additional neutron in the shell.

The calculated γ yields agree well with the experimental data, except in ^{6}Li and ^{14}C. However, even for these two nuclei the theory correctly reproduces the main facts—in the first nucleus the γ yield is maximal and in the second it is minimal. The strong discrepancy between theory and experiment in ^{14}C may also be due to the use of incorrect values of the mesoatomic parameters. The necessary experimental data are not available. The corresponding quantities were taken to be the same as in ^{12}C. However, as can be seen from Table VI of Ref. 1, there are already differences between the parameters in ^{12}C and ^{13}C.

The total γ yield calculated with the CK+ COP wave functions is very nearly equal to the CK+ MK yield. The initial nuclear ground state was always described using the CK parameter set. Thus, the total rate of the (π, γ) reaction hardly depends on the choice of the model parameters.

The good agreement between the calculated and measured total γ yields is not all that significant, since the theory has a number of weak points. First, there is the uncertainty in the values of the mesoatomic parameters. Second, the calculations do not take into account the contribution of spin-quadrupole transitions. Third, no allowance is made for the correlations in the ground state associated with transition of a nucleon to the band of $2\hbar\omega$ excitations.

The employed approach overestimates, as a rule, by about 1.5 times the probability of dipole transitions in the photodisintegration and μ-capture reactions in the $1p$ nuclei. There must be a similar overestimation of the rate for the (π, γ) reaction. With regard to the spin-quadrupole transitions, their contribution has been calculated[17] only in ^{16}O. Note that these transitions are important for pion capture from p orbits. With decreasing atomic number, the contribution of the transitions from the p orbits becomes weaker. Therefore, so do the spin-quadrupole transitions.

TABLE II. Calculated γ yields in the (π, γ) reaction associated with the $1\hbar\omega$ excitation ($T_f = T_i + 1$). For $A = 6$ the wave functions are taken from Ref. 14; for $A = 7$–15 the COP interaction was used (see the text).

Nucleus	J_i^π	J_f^π	Number of states	R_s	R_p	R (in 10^{-3})	Nucleus	J_i^π	J_f^π	Number of states	R_s	R_p	R (in 10^{-3})
^{6}Li	1$^+$	0$^-$	7	1.4	0.4	1.8	^{13}C	1/2$^-$	1/2$^+$	44	0.4	2.0	2.5
		1$^-$	14	5.6	3.4	9.0			3/2$^+$	67	1.3	5.3	6.6
		2$^-$	15	6.4	3.9	10.3			5/2$^+$	64	0.8	4.8	5.7
		3$^-$	8	1.8	2.1	3.9			7/2$^+$	44	0.0	0.3	0.3
		4$^-$	3	0.0	0.1	0.2			9/2$^+$	22	0.0	0.2	0.2
	Sum		47	15.2	9.9	25.2		Sum		241	2.5	12.6	15.3
^{7}Li	3/2$^-$	1/2$^+$	17	1.9	1.4	3.3	^{14}C	0$^+$	0$^-$	5	—	0.5	0.5
		3/2$^+$	24	3.3	2.8	6.1			1$^-$	13	0.9	4.1	5.0
		5/2$^+$	20	4.6	4.3	8.9			2$^-$	14	1.1	7.9	9.0
		7/2$^+$	10	0.6	0.9	1.5			3$^-$	10	0	0.2	0.2
		9/2$^+$	3	0.1	0.5	0.6			4$^-$	5	0	0.3	0.3
	Sum		74	10.5	9.9	20.4		Sum		47	2.0	13.0	15.0
^{9}Be	3/2$^-$	1/2$^+$	54	1.2	1.0	2.2	^{14}N	1$^+$	0$^-$	19	0.2	0.5	0.6
		3/2$^+$	82	1.5	1.4	2.8			1$^-$	45	0.7	3.0	3.7
		5/2$^+$	77	2.6	2.1	4.7			2$^-$	53	1.2	5.2	6.4
		7/2$^+$	50	1.1	1.1	2.2			3$^-$	41	0.8	5.9	6.7
		9/2$^+$	24	0	0.1	0.1			4$^-$	24	0	0.5	0.5
	Sum		287	6.4	5.7	12.0		Sum		182	2.9	15.1	17.9
^{11}B	3/2$^-$	1/2$^+$	77	0.5	1.7	2.2	^{15}N	1/2$^-$	1/2$^+$	8	0.4	1.6	2.0
		3/2$^+$	119	0.8	3.1	3.9			3/2$^+$	11	1.2	5.1	6.3
		5/2$^+$	117	1.3	4.6	5.9			5/2$^+$	10	1.0	7.4	8.4
		7/2$^+$	82	0.6	2.9	3.5			7/2$^+$	5	0	0.6	0.6
		9/2$^+$	44	0	0.2	0.2			9/2$^+$	2	0	0.4	0.4
	Sum		439	3.2	12.5	15.7		Sum		36	2.6	15.1	17.7

The contributions of the final states with different spin values J_f to the γ yields $R(J_f)$ for pion capture from different mesoatomic orbits are given in Table II for $1\hbar\omega$ transitions in $1p$-shell nuclei. The ratios between the yields are not determined by the numbers of final states. At the beginning of the $1p$ shell, the main contribution to the γ yield is made by transitions with $\Delta J = 0$ and 1; the contribution of the $\Delta J = 2$ transitions is small. As the $1p$ shell is filled, the contribution of the $\Delta J = 2$ transitions increases and that of the $\Delta J = 0$ transitions decreases. In nuclei at the end of the $1p$ shell the $\Delta J = 2$ transitions are comparable in intensity with the $\Delta J = 1$ transitions and even begin to exceed them slightly. The reason for the weakness of the $\Delta J = 2$ transitions at the beginning of the $1p$ shell will be discussed somewhat later in the part in which we consider particular nuclei. For the time being, we note that in nuclei for which the spin of the ground state is nonzero the $\Delta J = 2$ transitions are due to the action of the operator (1a) alone, whereas the $\Delta J = 1$ transitions are due to both (1a) and (1b). The high $\Delta J = 1$ intensity is related to this.

In contrast to the total rate, the partial rates are sensitive to the choice of the nuclear wave functions. The greatest sensitivity is in the cases when large components of the nuclear wave function are suppressed by the selection rules. Such a situation is realized, for example, in the isovector transitions of magnetic dipole type in a number of odd $1p$ nuclei. This makes it possible to use radiative pion capture as a probe for selecting model wave functions.

TABLE III. Measured and calculated partial γ yields (references are indicated by square brackets).

Nucleus	J_i	J_f	E_f^*, MeV	$R_{exp.}$, 10^{-4}	$R_{theor.}$, 10^{-4}
^{7}Li	3/2⁻	3/2⁻	0	1.94±0.30 [22]	4.5 [24]
^{9}Be	3/2⁻	3/2⁻	0	2.28±0.29 [22]	2.38 [24]
		1/2⁻	2.69	1.12±0.23 [22]	0.19 [24]
			4.31	0.19±0.45 [22]	1.80 (3/2⁻; 4.9 MeV) [24]
^{10}B	3⁺	0⁺	0	2.02±0.17 [22] 2.5±0.4 [6]	2.3 [24] 3.6 [6]
		2⁺	3.37	4.65±0.30 [22] 4.4±0.7 [6]	5.7 [24] 8.5 [6]
		2⁺	5.96	7.48±0.45 [22] 10.5±1.3 [6]	17.9 [24] 16.9 [6]
		3⁻	7.37	0.78±0.24 [22]	0.96 [24] 6.5 [6]
		2⁺	7.54	6.5±1.0 [6]	
		2⁺	9.4	2.17±0.40 [22]	1.5 [24]
^{11}B	3/2⁻	1/2⁺	0	2.98±0.33 [22]	0.70 [24] 0.80 [25]
		1/2⁻	0.32		3.6 [24]
^{12}C	0⁺	1⁺	0	6.22±0.35 [22]	6.8 [24] 8.4 [8]
		2⁺	0.95	1.29±0.25 [22]	3.5 [24] 4.9 [8]
^{13}C	1/2⁻	3/2⁻	0	6.08±1.2 [23]	12.9 [24]
^{14}N	1⁺	0⁺	0	0.25±0.11 [22] 0.3±0.2 [6]	0.9 [24]
		2⁺	7.01	6.2±0.4 [22] 7.7±0.9 [6]	
		2⁺	8.32	3.37±0.35 [22] 4.0±0.6 [6]	20.6 [24] 24.4 [6]

Table III gives the partial γ yields in the case of pion capture by the nuclei ^{7}Li, ^{9}Be, $^{10\,11}$B, $^{12\,13}$C, and ^{14}N. The table includes transitions to the ground and low-lying states of the final nuclei. Deferring discussion of the degree of quantitative agreement between theory and experiment, we note that the transitions are weak to the ground states of the daughter nuclei in the case of pion capture by ^{7}Li, ^{9}Be, ^{10,11}B, and ^{14}N. In ^{6}Li, ^{10}B, ^{12,13}C, and ^{14}N at low excitation energies the strongest transitions are those that populate the states (or, more probably, their analogs) which form the magnetic dipole resonance in the initial nucleus. It is in these nuclei that the $M1$ resonance is most clearly manifested in electron scattering.

Thus, the microscopic approach to nuclear structure can describe the experimentally observed excitation of the low-lying states of $1p$ nuclei. The agreement with experiment can be significantly improved by more careful construction of the wave functions. Such examples are available for nuclei of the $2s$–$1d$ shell,[26,27] for which correct values of the magnetic moments have been obtained. For this, the wave functions were constructed in a complete basis in the $0\hbar\omega$ excitation band and renormalized single-particle orbital and spin angular momenta were introduced. The available data on the (π,γ) reaction in the $2s$–$1d$ nuclei also agree with the results of calculation on the basis of such functions.[28]

Magnetic dipole $M1$ resonance

The examples considered above indicate very clearly excitation of the $M1$ resonance in light nuclei as a result of radiative pion capture. Of course, these strong isovector $M1$ resonances had already been observed, especially in electron scattering with small momentum transfer.[29-32] For the $2s$–$1d$ nuclei ^{20}Ne, ^{28}Si, and ^{32}S the data on radiative pion capture[23,33] are also correlated with the data on inelastic electron scattering. In nuclei with $A>32$, magnetic dipole transitions are not so clearly manifested in radiative pion capture.

Inelastic electron scattering with high resolution remains an important source of information about transitions of this type. Recently, much information[34,35] about $M1$ transitions has been obtained by investigation of the charge-exchange (p,n) reaction. The resonances excited in this reaction have become known as Gamow–Teller resonances. The observation of these resonances in the magic nuclei ^{40,48}Ca and ^{16}O directly indicates the existence of nucleon correlations in the ground state.[36] This question was discussed in detail in Ref. 1. The strength of the corresponding transitions yields information about the repulsive part of the effective spin–isospin nucleon–nucleon potential. In Migdal's theory, it is determined by the parameter g'. All these questions are very topical and are under intense discussion.

In a discussion of $M1$ transitions in $1p$ nuclei, it is expedient to proceed from the fact that a supermultiplet level scheme is realized approximately in these nuclei. Because of this, one can separate a dominant component in the wave function that determines the main characteristics of the transition.

In the $1p$ nuclei, the strongest $M1$ transitions are as follows:

^{6}Li : $J^\pi T = 1^+0 \to 0^+1$; $E^* = 3.56$ MeV;
^{10}B : $J^\pi T = 3^+0 \to 2^+1$; $E^* = 7.48$ MeV;
^{12}C : $J^\pi T = 0^+0 \to 1^+1$; $E^* = 15.1$ MeV;
^{13}C : $J^\pi T = 1/2^-1/2 \to 3/2^-3/2$; $E^* = 15{,}1$ MeV;
^{14}N : $J^\pi T = 1^+0 \to (2^+1)_1$; $E^* = 9.17$ MeV and $(2^+1)_2$; $E^* = 10.43$ MeV.

They are revealed in electron scattering, and their analogs in (π,γ), (μ,ν), and some other reactions. The analysis of these strong $M1$ transitions shows that they are predominantly due to the spin–isospin component of the electric current $\tau\sigma$.[37] For example, in the ^{12}C nucleus the fraction of the latter is about 95%. Decomposition of the total matrix element of the electromagnetic $M1$ transition into spin and orbital components is also possible without the use of model wave functions if one analyzes simultaneously the γ transitions, β decay, and (π,γ) reaction. The last two are due to purely spin operators. In nuclei of the $2s$–$1d$ shell there are a number of examples when the two components of the electromagnetic current make comparable contributions to the $M1$ amplitude.[27,38] One of the examples is associated with ^{20}Ne. We shall discuss it below in Sec. 2.

Measurements of the cross sections for electron scattering through large angles ($\theta = 180°$) at small momentum transfers yield information about the distribution of the particles over the various single-particle states and, in particular, over the states that are spin–orbit doublets: $j_> = l + \frac{1}{2}$ and $j_< = l - \frac{1}{2}$. Under the influence of the magnetic dipole perturbation there are strong transitions between such states, especially if the momentum transfer is small, when we have the so-called *photon point* ($q \sim E^*$, where E^* is the energy of the lev-

el). Varying the momentum transfer, one can also obtain information the relative importance of the spin and orbital components of the electromagnetic current.[32]

In discussing the $M1$ transitions, we concentrate our main attention on how their manifestation in the (π,γ) reaction is related to the structure of the nuclear states and, in particular, realization of a supermultiplet scheme. In the low-energy limit (photon point), the component $\tau_-\sigma$ of the transition operator couples the initial (ground) state $|[\lambda_0](L_0S_0)J_0T_0\rangle$ of the nucleus to final states $|[\lambda](LS)JT\rangle$ in which the Young tableau $|\lambda|$ characterizing the symmetry of the orbital part of the function does not change and for the remaining quantum numbers there are the selection rules

$$\Delta L = 0;\quad \Delta S = 1 \text{ and } 0;\quad \Delta J = 1 \text{ and } 0;\quad \Delta T = 1,$$

which follow from the rules of vector addition. These rules work in such a way that strong $M1$ transitions are realized in the odd–odd nuclei ^{6}Li, ^{10}B, and ^{14}N, while they are weak in the odd–even ^{7}Li, ^{9}Be, and ^{11}B. In ^{12}C and ^{13}C a strong $M1$ transition is also observed, but it proceeds because of the strong deviation from the supermultiplet scheme, which is maximal in the nuclei in the middle of the $1p$ shell. When the momentum transfer is shifted from the photon point to $q\sim m_\pi$, the picture of excitation of the $M1$ resonance hardly changes (Fig. 1).

Information about the discussed Gamow–Teller transitions is also contained in the cross sections of the (p,n) and (n,p) charge-exchange reactions when the incident particle has energy from 100 to 200 MeV and the scattered particle is detected at a small angle (Fig. 2). The results of such measurements can be analyzed in detail in $1p$ nuclei. Using the results of such analysis, one can then turn to heavier nuclei, in which the situation with regard to the magnetic transitions is less clear and the (e,e') reaction is not so informative.[42,43]

We now turn to a detailed discussion of $M1$ transitions in nuclei of the $1p$ shell.

Odd–Odd Nuclei. ***Nuclei with*** $A = 6$ ***and*** 14. The orbital angular momentum of the dominant component of the ground-state wave function of the ^{6}Li and ^{6}He nuclei is zero ($L = 0$), and the orbital symmetry $[\lambda] = [2]$ is maximal:

$$^6\text{Li}: |1^+0\rangle = \alpha\,|1p^2\,[2]^{13}S_1\rangle + \ldots,\ 0.92 \leqslant \alpha \leqslant 0.99 \qquad (3)$$

$$^6\text{He}: |0^+1\rangle = \beta\,|1p^2\,[2]^{31}S_0\rangle + \ldots,\ 0.88 \leqslant \beta \leqslant 1.00. \qquad (4)$$

To classify the wave functions with respect to the orbital angular momentum L, the spin S, the isospin T, and the orbital Young tableau $[\lambda]$ we use in (3) and in what follows the standard notation $[\lambda]^{2T+1\,2S+1}L_J$. The spatial parts of the wave functions (3) and (4) completely overlap and the strength of the $M1$ transition at small momentum transfers is concentrated on a single (the ground) state of ^{6}He.

The lowest ^{6}He state with spin $J^\pi = 2^+$ is also described by a function with maximal orbital symmetry. It has excitation energy $E^*(^6\text{He}) = 1.8$ MeV, which corresponds to $E^*(^6\text{Li}) = 5.37$ MeV. The orbital angular momentum is $L = 2$ (see Table X in Sec. 3):

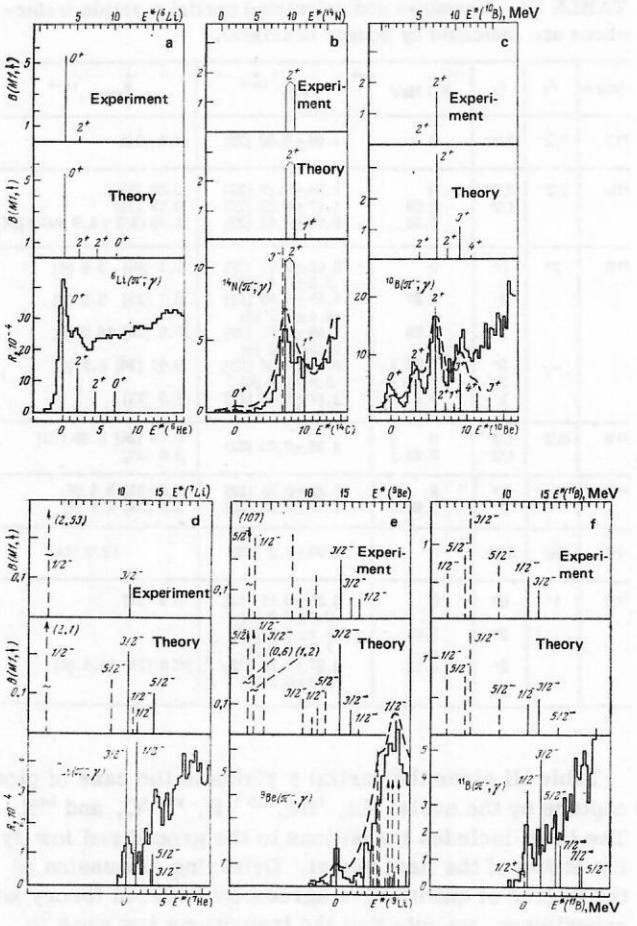

FIG. 1. Probabilities $B(M1)$ of electromagnetic ($q=\omega$) and (π, γ) transitions in the nuclei ^{6}Li (a), ^{14}N (b), ^{10}B (c), ^{7}Li (d), ^{9}Be (e), and ^{11}B (f). The broken curves are the theoretical results obtained under the assumption that each resonance has Breit–Wigner shape and width 2 MeV; the experimental values of $B(M1)$ are taken from Ref. 39, and the units are (nuclear magnetons)^2; the histograms are taken from Refs. 40 and 41; the broken lines for $B(M1)$ correspond to transitions with $\Delta T = 0$; the broken lines for the (π, γ) reaction correspond to $1\hbar\omega$ transitions.

$$|2^+1\rangle = \alpha_2\,|[2]^{31}D_2\rangle + \beta_2\,|[11]^{33}P_2\rangle, \qquad (5)$$

where $\alpha_2 \approx 0.97$. Therefore, in the long-wave approximation (photon point) the excitation of this state in $M1$ transitions is due solely to admixtures of components as in (5) and in (3). When $q\sim m_\pi$, an additional transition strength is concentrated on this level by virtue of the operator $j_2(qr)\,[\sigma\otimes Y_2]$, and for the (π,γ) reaction by virtue of the operator $rj_1(qr)\,[\sigma\otimes Y_2]$ as well. A quantitative analysis of the transition rates to these two levels will be made below.

The $J^\pi T = 1^+1$ level of ^{6}He is also weakly excited as a result of the $M1$ transition, since its structure is determined by the function $|1p^2\,[11]^{33}P_1\rangle$, for which the spatial part is completely antisymmetric.

In ^{14}N, the situation is somewhat different. In the ^{14}N ground-state wave function the dominant component has $L = 2$ (see, for example, Ref. 44):

$$^{14}\text{N}: |1^+0\rangle = 0.95\,|1p^{10}\,[442]^{13}D_1\rangle - 0.25\,|[433]^{11}P_1\rangle - 0.20\,|[442]^{13}S_1\rangle. \qquad (6)$$

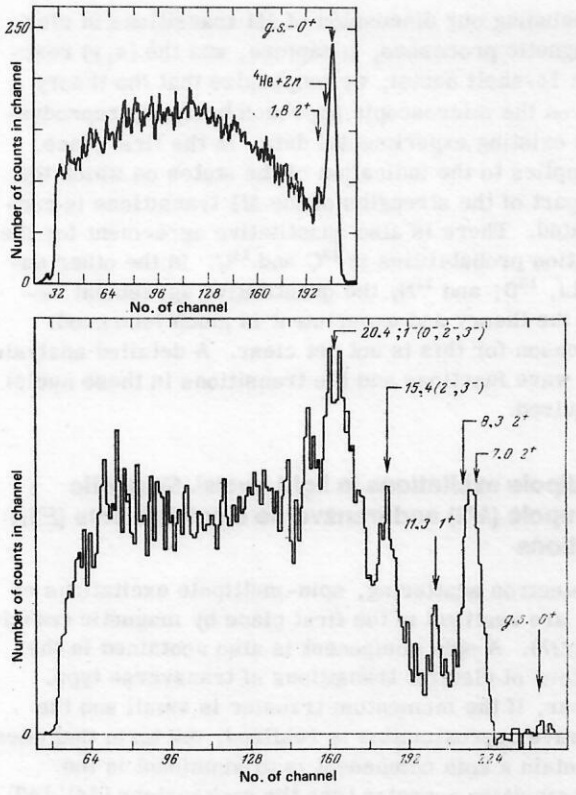

FIG. 2. Cross section of the (n, p) charge-exchange reaction. The momentum transfer is the same as in the (π, γ) reaction. The upper part of the figure corresponds to the reaction $^6\mathrm{Li}(n, p)^6\mathrm{He}$ ($E_n = 56.3$ MeV, $\theta_{\mathrm{lab}} = 10°$); the lower part corresponds to $^{14}\mathrm{N}(n, p)^{14}\mathrm{C}$ ($E_n = 59.1$ MeV, $\theta_{\mathrm{lab}} = 18°$).[42]

In the limit $q \to 0$, the $M1$ transition to the ^{14}C ground state, whose wave function has the form

$$^{14}\mathrm{C}: |\, 0^+1\rangle = 0.75\, |\, 1p^{10}\, [442]^{31}S_0\rangle + 0.66\, |\, [433]^{33}P_0\rangle, \qquad (7)$$

is due solely to the components of the ^{14}N wave function for which $L = 0$ and 1. As was noted long ago, in this transition there is a mutual suppression of the contributions of the components with different L values. The transition rates for β decay as well as for electron scattering, etc., change appreciably when one includes the noncentral component of the residual nucleon–nucleon interaction and meson exchange currents.[45]

In the (π, γ) reaction, the transition to the ^{14}C ground state is also weakly manifested. Its rate is basically determined by the matrix elements of the operators $j_2(q\gamma)\,[\sigma \otimes Y_2]_1$ and $\gamma j_1(q\gamma)\,[\sigma \otimes Y_2]_1$, which are small. Because the main matrix element of the operator $\tau\sigma$ is suppressed, the (π, γ) transition makes it possible to investigate effects associated with various corrections to the Hamiltonian. It was from this point of view that the $^{14}\mathrm{N}(\gamma, \pi)^{14}\mathrm{C}$ reaction was analyzed in Ref. 46.

The strength of the isovector $M1$ transitions in ^{14}N is found to be concentrated on the level $J^\pi T = 2^+1$, whose wave function has the form

$$|\, 2^+1\rangle = \alpha\, |\, 1p^{10}\, [442]^{31}D_2\rangle + \ldots, \qquad (8)$$

where $\alpha \approx 0.90$. The overlapping of the orbital part of this function with the orbital part of the ^{14}N ground-state function is almost complete. However, as follows from the experimental electron scattering data,[47] the strength of the $M1$ transitions is distributed over two levels with spin $J^\pi = 2^+$: with energy $E^x(^{14}\mathrm{N}) = 9.17$ MeV and $E^x(^{14}\mathrm{N}) = 10.43$ MeV. In the (π, γ) reaction, these two levels are also excited.[41,48] In Ref. 24, in contrast to Ref. 6, a large contribution to the γ yield is predicted in the same energy region from the $J^\pi = 3^-$ level. The excitation of this level is due mainly to the $M2$ transition. There is an indication[49] of manifestation of the $J^\pi = 3^-$ level in μ capture (however, see Ref. 50).

The investigation of μ capture has also revealed preferred excitation of the $J^\pi = 2_1^+$ level in ^{14}C. The transition rate was found[50] to be $\Lambda_\mu = 4640 \pm 740$ sec^{-1}, which is somewhat less than expected in the theory of Refs. 3 and 51. In the (n, p) charge-exchange reaction the $J^\pi T = 2^+1_1$ level can also be clearly seen[42] (see Fig. 2). With regard to the $J^\pi T = 1^+1$ level, it is weakly excited, as in ^{6}Li, since the orbital symmetry [433] of the corresponding state differs from the symmetry of the dominant component of the ground-state wave function.

$A = 10$. In contrast to ^{6}Li and ^{14}N, the strength of the isovector $M1$ transitions in ^{10}B is distributed over several states.[41,48] The theory also predicts such an effect.[24] Despite the large statistical weight, the resonances with spins $J = 3$ and 4 are excited less strongly than the resonance with spin $J = 2$. This is due to the supermultiplet structure of the levels.

The ^{10}B ground-state wave function is basically a superposition of components whose orbital angular momentum is $L = 2$ (Ref. 44):

$$|\, 3^+0\rangle = \sum \alpha_i\, |\, 1p^6\, [42]^{13}D_3^{(i)}\rangle + \ldots. \qquad (9)$$

They differ only in the seniority quantum number. The levels with spin and parity $J^\pi = 3^+$ and 4^+ and maximal spatial symmetry [42] are described by components with angular momentum different from 2. The state with $J^\pi T = 3^+1$ has dominant component $[42]^{31}F_3$, and the state with $J^\pi T = 4^+1$ has the component $[42]^{31}G_4$. It follows that only states with $J^\pi T = 2^+1$ will be populated as a result of $M1$ transitions. There are two such states:

$$|\, 2^+1\rangle_1 = 0{,}73\, |\, [42]\, ^{31}D_2^{(1)}\rangle + 0{,}21\, |\, [42]\, ^{31}D_2^{(2)}\rangle + \ldots; \qquad (10)$$

$$|\, 2^+1\rangle_2 = -0{,}23\, |\, [42]\, ^{31}D_2^{(1)} + 0{,}89\, |\, [42]\, ^{31}D_2^{(2)}\rangle + \ldots. \qquad (11)$$

In the first case, there is destructive interference of the matrix elements; in the second, constructive. The μ-capture data also indicate preferred excitation of the $J^\pi T = (2^+1)_2$ state:

$$R_\mu = \Lambda_\mu(3^+ \to 2_1^+)/\Lambda_\mu(3^+ \to 2_2^+)$$
$$= (390 \pm 960)\,\mathrm{sec}^{-1}/(4710 \pm 705)\ \mathrm{sec}^{-1} = 0.08 \pm 0.20. \qquad (12)$$

The theory of Ref. 51 predicts a larger value for R_μ:

$$R_\mu = 0.33. \qquad (13)$$

For the (π, γ) reaction too the theory predicts a ratio close to (13): $R(2_1^+)/R(2_2^+) = 0.32$ in accordance with Ref. 24 and 0.50 in accordance with Ref. 6. The experiments give the values 0.62 ± 0.04 (Ref. 22) and 0.42 ± 0.08 (Ref. 6).

The ^{10}Be ground state, whose wave function has the structure[44]

$$|0^+1\rangle = 0.77\,|[42]^{31}S_0\rangle - 0.48\,|[411]^{33}P_0\rangle + \ldots, \quad (14)$$

is excited by $M3$ transitions. The relative distribution of the (π,γ) transition intensities to the ground and low-lying excited states is basically reproduced by the theory using wave functions (variant MK) (see Table III) and in the phenomenological approach.[48,52] The results of the phenomenological approach will be discussed below.

The Even–Even Nucleus ^{12}C. The isovector $M1$ transition in the even–even self-conjugate nucleus ^{12}C is characterized by relatively weak overlapping of the spatial parts of the wave functions. The principal component of the ^{12}C ground-state wave function has the maximal spatial symmetry [44]. The wave function of the resonance state cannot contain a component with such symmetry. The maximal symmetry in this case is [431]. Nevertheless, the $M1$ transition in ^{12}C is as strong as in the odd–odd nuclei, and is a classical example of concentration of strength on a single level. The electromagnetic $M1$ transition in ^{12}C is associated with a component with Young tableau [431] (and orbital angular momentum $L = 1$) which occurs in the ground-state [44] wave function:

$$^{12}\mathrm{C}: |0^+0\rangle = 0.85\,|1p^8\,[44]^{11}S_0\rangle + 0.50\,|[431]^{13}P_0\rangle + \ldots \quad (15)$$

with weight 25%. The corresponding Young tableau in the wave function of the resonance $J^\pi T = 1^+1$ ($E^* = 15.11$ MeV in ^{12}C),

$$|1^+1\rangle = 0.86\,|1p^8\,[431]\,^{33}P_1\rangle + 0.33\,|[422]\,^{33}S_1\rangle, \quad (16)$$

is manifested in the first component.

In the (π,γ) reaction, the operator $[\sigma\otimes Y_2]$ also contributes to the transition to the corresponding analog state (^{12}B ground state).

Odd Nuclei. In nuclei with odd A (^{7}Li, ^{9}Be, and ^{11}B) the $M1$ transitions are suppressed, owing to the weak overlapping of the spatial parts of the wave functions—the main components of the initial and final states have different Young tableaux. In these nuclei, the electromagnetic $M1$ transitions to levels with the same isospin as the ground state ($\Delta T = 0$ transition) are even stronger than to levels with $T_f = T_i + 1$ ($\Delta T = 1$ transition).

In radiative pion capture by ^{7}Li, ^{9}Be, and ^{11}B nuclei the partial transitions to negative-parity low-lying states also have low intensity.[48,53] As follows from the calculations of Refs. 3, 51, and 54, the situation is similar for μ capture.

In ^{13}C, a strong $M1$ transition is already observed[23,55] to a level with $T = 3/2$ in the (π,γ) reaction and in electron scattering, which agrees well with the theory. In both ^{12}C and ^{13}C there is a strong deviation from a supermultiplet structure of the levels—the ground-state wave function contains a ~25% admixture of the configuration with a less symmetric Young tableau: [431] in ^{12}C and [432] in ^{13}C. Because of these components, the $M1$ transition in the carbon isotopes is strong.

Concluding our discussion of $M1$ transitions in electromagnetic processes, μ capture, and the (π,γ) reaction in $1p$-shell nuclei, we emphasize that the theory based on the microscopic approach basically reproduces the existing experimental data. In the first place, this applies to the indication of the states on which the main part of the strengths of the $M1$ transitions is concentrated. There is also quantitative agreement for the transition probabilities in ^{12}C and ^{13}C. In the other nuclei ^{6}Li, ^{10}B, and ^{14}N, the quantitative agreement between the theory and experiment is much less good. The reason for this is not yet clear. A detailed analysis of the wave functions and the transitions in these nuclei is required.

Spin-dipole excitations in light nuclei. Magnetic quadrupole ($M2$) and transverse electric dipole ($E1t$) transitions

In electron scattering, spin-multipole excitations of nuclei are realized in the first place by magnetic transitions ($M\lambda$). A spin component is also contained in the operators of electric transitions of transverse type. However, if the momentum transfer is small and the long-wave approximation is realized, the term that does not contain a spin component is predominant in the ($E\lambda t$) transition operator (see the expressions (44)–(47) of Ref. 1). In the region of momentum transfers of order 100 MeV/c and above, the spin component of the $E1t$ operator becomes dominant.

The available experimental data on spin transitions of multipolarity $\lambda > 1$ are rather sparse. An appreciable concentration of the $M2$ transition strengths is observed in large-angle electron scattering in only a few nuclei.[31,32] There are indications of $E1t$ excitations in ^{12}C.[31,56] In heavy nuclei, the observed strength of the $M2$ transitions is much less than is predicted by theory, i.e., there is suppression of the spin component of the current.[57]

Configuration Splitting of Spin-Dipole Resonances in $1p$-Shell Nuclei. In Sec. 6 of Ref. 1 and in Refs. 58 and 59 it was shown that basically the strength of the $M2$ transitions must be weakly concentrated, and various reasons for this effect were given. They are related both to the weakness of the spin-dependent residual nucleon–nucleon interaction in the nucleus and the large energy spread of the undisturbed configurations. Thus, in the $1p$ nuclei the unperturbed energies of the single-particle states forming the $M2$ resonance are spread over an energy interval of 10 MeV (see Table XIII in Ref. 1). The spin–orbit interaction facilitates this large spread. In light nuclei, there is one further source of spreading—the so-called *configuration splitting*.[59] It is due, first, to the manifestation in light nuclei of a "fouring" of nucleons (the binding energy of a nucleon is greater if its stripping breaks up a filled row of the orbital Young Tableau) and, second, to the fact that the binding energy of a nucleon of a closed shell that participates in a dipole transition increases fairly rapidly with increasing number of particles in the outer unfilled shell, whereas the binding energy of a nucleon on the Fermi surface, which is where the nucleon from

the closed shell arrives, remains approximately constant.

The residual interaction of the nucleons in the nucleus is not capable of bringing together in a single peak such widely spaced single-particle excitations, and therefore the $M2$ resonance is formed from several peaks.[60,61] With regard to the $E1t$ transitions, they are localized in a narrower energy interval, although there is also configuration splitting for them.[60,61]

Because of the configuration splitting in light nuclei, there are two or more peaks in the photoabsorption spectra even in electric dipole ($E1$) transitions. Thus, in $1p$ nuclei the high-energy region is resonantly coupled to the excitation of nucleons of the closed $1s$ shell, and the low-energy region is coupled to the excitation of nucleons of the $1p$ shell. Such splitting also occurs in the (π,γ) reaction[60,61] for $M2$ and $E1t$ transitions. The structure of the γ spectrum in the (π,γ) reaction in nuclei of the $1p$ shell as well as the region of localization of the transitions and the mean excitation energy of the nucleus are determined by the configuration splitting. The excitation intensity of a particular energy region is related to the degree of filling of the outer shell. The nature of the decay of resonances is also associated with the configuration splitting.[59]

The $M2$ excitations in the $1p$ nuclei are associated with strong single-particle transitions: $1p_{3/2} \to 1d_{5/2}$ and $1s_{1/2} \to 1p_{3/2}$; the transverse $E1$ excitations, with their spin–orbit partners: $1p \to 1d_{3/2}$ and $1s_{1/2} \to 1p_{1/2}$. Because of this, the concentration of the $E1t$-transmission strengths in the $1p$ nuclei occurs at higher excitation energies of the nuclei than it does for the $M2$ transitions. Moreover, the configuration splitting is damped more weakly in the $E1t$ transitions as the $1p$ shell is filled, since the $1p_{1/2}$ subshell is filled last. Thus, in the region of high excitations of the nuclei associated with the $1s \to 1p_{1/2}$ transition there is always a shoulder in the nuclei of the $1p$ shell. As the $1p$ shell is filled, the position of the $M2$ resonance will be shifted to lower excitation energies of the nucleus, and the region of its localization will become narrower. This tendency is confirmed in the observed radiative-pion-capture spectra. These features of the spin excitations of the $1p$ nuclei can be clearly followed in the calculated curves in Figs. 3 and 4.

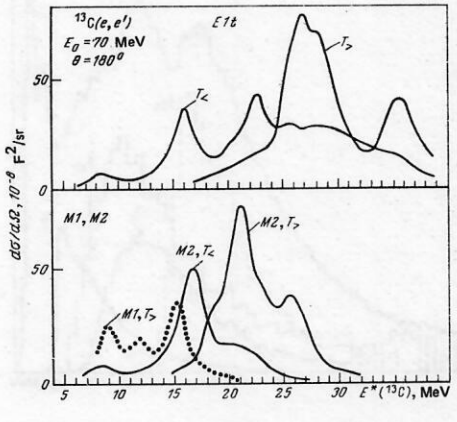

FIG. 3. Spin-monopole and spin-dipole transitions in the ^{13}C nucleus predicted by theory in the framework of the shell model.

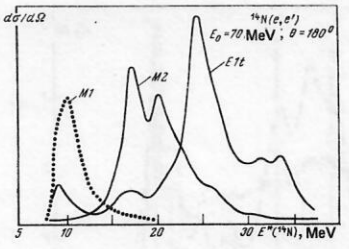

FIG. 4. Spin-monopole and spin-dipole transitions in the ^{14}N nucleus predicted by theory in the framework of the shell model.

The available data on the (π,γ) reaction are fairly extensive, especially in the region of the $1p$ nuclei. On the basis of these data, we can systematize the accumulated material and establish the main features of the nuclear transitions due to $M2$ and $E1t$ excitations. We can then make deliberate searches for such transitions in other reactions. We analyze in detail the $M2$ and $E1t$ transitions in light nuclei in the (π,γ) reaction, using the shell model. In such an approach, as will be shown below, one can explain the main features of the excitation of $1p$ nuclei in the (π,γ) reaction. It should be emphasized that in a number of cases, for example, in ^{13}C and ^{14}C, the theoretical results preceded the experimental ones.

Specific Nuclei. ***The*** ^{6}**Li** ***Nucleus.*** The γ spectra of radiative pion capture by ^{6}Li has two broad maxima. The centroid of one is at the excitation energy $E^* = 15$ MeV in the intermediate nucleus ^{6}He, and the other is at the energy $E^* = 25$ MeV (Fig. 5). This structure of the spectrum can be traced for capture of not only pions from the $1s$ orbit of the pionic atom but also from a superposition of states. Besides the two broad peaks, there is also one narrow peak, which corresponds to concentration of the $M1$-transition strengths.

Analysis of the ^{6}Li excitation in the (π,γ) reaction made in the framework of the shell model[18,63] showed that the maximum in the region of excitation $E^* = 15$ MeV of the ^{6}He nucleus is associated with transition of a nucleon of the valence shell with the formation of states described by the configuration

$$|1p^1,(2s \text{ or } 1d)^1 : {}^{33}L_J\rangle. \qquad (17)$$

In the same energy region there are localized transitions of a nucleon from the $1s$ shell leading to formation of states with Young Tableau [33]:

$$|\, 1s^{-1},\ 1p^3\ [3]^{22}P : {}^{33}P_J\,\rangle. \qquad (18)$$

It is these states that decay through the ^{3}He + ^{3}H channel. This channel is already distinguished in the μ-capture reaction, as is its analog in the photodisintegration reaction (see Ref. 59).

The resonances at higher excitation energy of the nucleus are formed as a result of transition of a nucleon from the $1s$ shell, but the symmetry of the wave functions of the corresponding states is not so high:

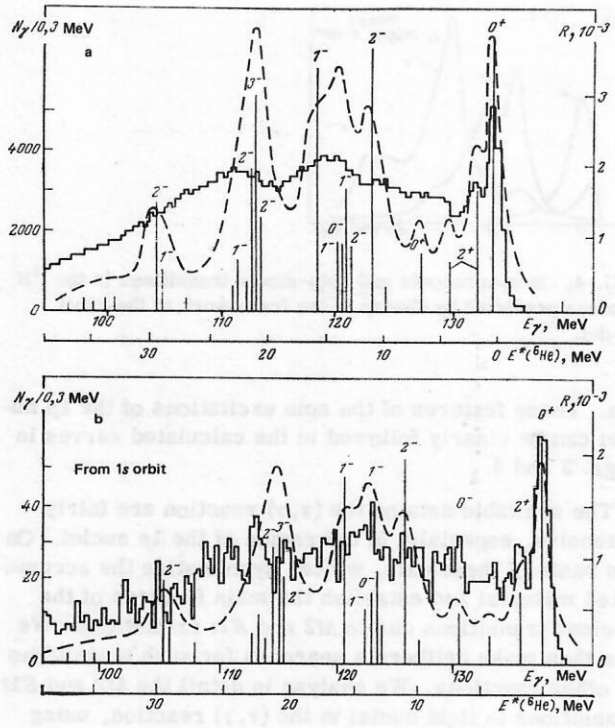

FIG. 5. The γ spectra[62] from the $^6Li(\pi, \gamma)$ reaction. The histogram gives the result of the measurements. The broken curve (relative units) is obtained from the calculated yields[18,63] (vertical lines, right-hand scale) under the assumption that each resonance has Breit–Wigner shape: a) total yield $R = R_s + R_p$; b) yield corresponding to capture from the $1s$ orbit.

$$|\, 1s^{-1},\ 1p^3\,[21]\rangle. \tag{19}$$

This group of states will undergo many-particle breakup, to $^3H + d + n$ or $^3H + 2n + p$, in complete analogy with the μ-capture and photodisintegration reactions.

It follows from the calculations that in the low-energy part of the excitation spectrum of the intermediate nucleus the transition intensities in the (π, γ) and photoabsorption reactions are too small. Experiment shows that this is not the case. The contradiction between the theory and experiment may be partly due to a raising of the positions of some of the calculated levels and partly to the fact that the width of the low-lying resonances is much greater than the width $\Gamma = 2$ MeV used in the calculation. Estimates using R-matrix theory give for the width $\Gamma = 5$–8 MeV.

In both the Li isotopes, additional selection rules arise because of the supermultiplet structure of their levels; these suppress the $\Delta J = 2$ transitions. Indeed, the ^6Li ground state is described basically by the component (3). The spin-dipole operator $\tau[\sigma \otimes Y_1]$ couples it only to the components

$$|\, 1p^1\,(2s \text{ or } 1d)^1 : {}^3P_J\,\rangle, \tag{20a}$$

$$|\, 1p^1\,(2s \text{ or } 1d)^1 : {}^1P_1\rangle, \tag{20b}$$

in which the orbital angular momentum takes the single value $L = 1$. Under such a condition, the total angular momentum of the system cannot exceed $J_f = 2$. But if the transition is associated with the excitation of a deep $1s$ nucleon, then for realization in the final state of the high symmetry

$$|\, 1s^{-1},\ 1p^3\,[3]^2P : {}^3P\rangle \tag{21}$$

the orbital angular momentum can again take only the one value $L = 1$ and the total angular momentum cannot exceed $J_f = 2$. For the states with the less symmetric configurations

$$|\, 1s^{-1},\ 1p^3\,[21]\,{}^2P : {}^3P_J\,\rangle; \tag{22a}$$

$$|\, 1s^{-1},\ 1p^3\,[21]\,{}^2P : {}^1P_1\rangle \tag{22b}$$

the total angular momentum of the nucleus also does not exceed two units. And only the one configuration

$$|\, 1s^{-1},\ 1p^3\,[21]\,{}^4P : {}^5P_J\,\rangle \tag{23}$$

is associated with excitation of a final state with total angular momentum $J_f = 3$. Thus, in the γ spectrum of the $^6Li(\pi, \gamma)$ reaction transitions to the levels $J^\pi = 2^-$ and 1^- must be predominantly manifested. The analogs of these states in ^6Li form the photonuclear resonance. The systematic calculation made in Ref. 63 completely confirmed the conclusions based on the qualitative arguments, namely, the excitation spectrum in the $^6Li(\pi, \gamma)$ reaction is formed by a series of transitions to the $J_f^\pi = 2^-$ levels ($\Delta J = 1$) and only one transition to a $J_f^\pi = 3^-$ level. The calculations of the dipole resonance in ^6Li on the basis of the cluster model lead to an analogous structure of the excitation spectrum (see Ref. 59).

We now compare the γ spectrum associated with radiative pion capture by the ^6Li and ^4He nuclei. From an energy of about $E_\gamma \approx 115$ MeV, the spectra appear to repeat each other (Fig. 6). There is a similar effect in the photonuclear reactions; from about $E_\gamma \approx 30$ MeV, the total photoabsorption cross sections repeat each other.[59,68] The similarity in the shape and intensity of the spectra is due to the fact that in this excitation region of the ^6Li nucleus the main contribution to the process is made by a $1s$ nucleon, i.e., a quartet of nucleons is broken up [see (22)]. In other words, the pro-

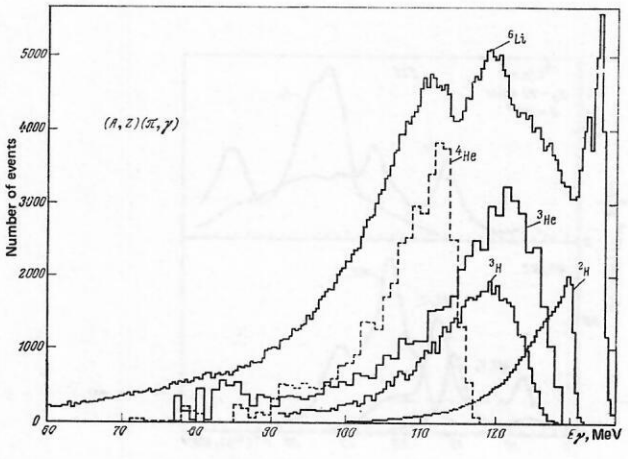

FIG. 6. The γ spectrum[62] from the $^6Li(\pi, \gamma)$ reaction compared with the γ spectra from the capture of pions by the nuclei ^4He (Ref. 64), ^3He (Ref. 65), ^3H (Ref. 66), and ^2H (Ref. 67).

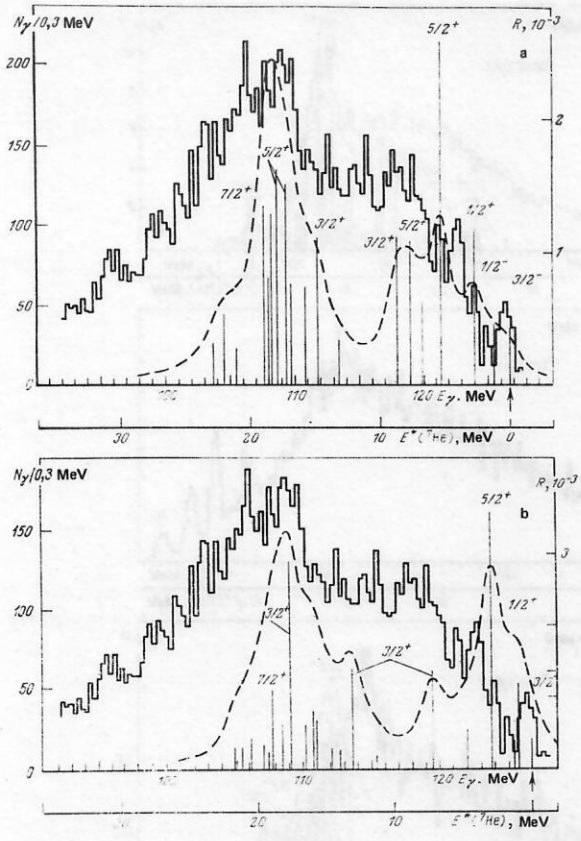

FIG. 7. The γ spectrum[24] from the $^7Li(\pi^-, \gamma)$ reaction. The calculation was made with the standard set of parameters (b) and with the MK set (a).[11]

cess in this case is associated with quasi-α-particle absorption.[40,62] Comparison of the γ spectra associated with radiative pion capture by ^{7}Li and ^{4}He also reveals their agreement at high excitation energies of the nuclear system. This again is due to the fact that a quartet of strongly coupled nucleons in the 1s shell comes into action (Fig. 7).

The hardest part of the γ spectrum in the $^6Li(\pi, \gamma)$ reaction corresponds to absorption of pions by the outer nucleons with the formation of states described by the configuration s^4p^2. This suggests an analogy with the (π, γ) reaction on the deuteron. But whereas the nuclear system in the deuteron reaction is in the continuous spectrum in the final state, for ^{6}Li the corresponding transition leads to a bound state. Hence the difference in the shape of the γ spectra in the case of radiative pion capture by ^{6}Li, the corresponding maximum being narrow and pronounced.

The maximum in the central region of the spectrum for radiative pion capture by ^{6}Li is formed by transitions to states described by the configurations (21). These states then decay through the $^3H + ^3H$ channel. Thus, the process proceeds as if on the three-particle subsystem ^{3}He. The three-nucleon system can be formed not only in the bound state, but can also decay into $d + n$ and $2n + p$.

The $^6Li(\pi, \gamma)$ reaction has also been studied in coincidence with mesic x-ray emission corresponding to a $2p \to 1s$ transition: $\Delta E(2p-1s) = 25$ keV. The coincidence method revealed a branch of radiative pion capture associated solely with pion absorption from the 1s orbit. The gross structure of the excitation spectrum of the nucleus for capture from only the 1s orbit and from different orbits is almost the same. This was also predicted by the theory. The difference between capture from the s and p orbits is due mainly to the difference in the excitation of states with $J^\pi = 3^-$, and the part they play in radiative pion capture by the ^{6}Li nucleus is, as we have already seen, not large.

Completing our discussion of the response of the ^{6}Li nucleus in the (π, γ) reaction, we note that a systematic study of the disintegration of this nucleus is complicated by the presence of many-particle channels. The theoretical analysis we have made should be regarded as qualitative and preliminary, its aim being to reveal the main features of the process.

The calculated γ spectrum is rather sensitive in its high-energy part to the details of the nuclear structure. Therefore, a systematic investigation is required in this part of the spectrum. Deeper understanding of the part played by the nuclear structure could be gained by investigating electron scattering with high resolution, the main photodisintegration channels with coincidence of emitted particles required, etc. (see the review of Ref. 59).

We also consider a theoretical interpretation of the response of the ^{6}Li nucleus in the (π, γ) reaction and in electron scattering. It is based on a single-particle representation of the process. Analysis of the $^6Li(\pi, \gamma)$ reaction showed that the single-particle model does not reflect the observed picture, except for the region of high excitation energies ($E^* \gtrsim 30$ MeV),[69] where the resonance effects are unimportant. In the single-particle approach, the $1s \to 1p$ transitions were concentrated in the low-energy region of ^{6}He. This is a typical result for such a model. Inclusion of the residual interaction between the nucleons leads to the states being pushed into the region of high excitation energies. After inclusion of the interaction, it is found, as we have seen, that it is precisely because of the $1s \to 1p$ transition that the maxima in the excitation spectrum are formed.

The ^{7}Li Nucleus. Both in photoabsorption and in radiative pion capture by the ^{7}Li nucleus the region of localization of the transitions is very broad.[53,70] This is due to the configuration splitting of the resonance.[18,59] In discussing the ^{7}Li response as a result of radiative pion capture, we shall again proceed from the approximate realization in this system of a supermultiplet level scheme. The broad maximum with centroid at excitation energy $E^*(^7He) = 15$ MeV corresponds to transitions of a 1s nucleon with the formation of states whose symmetry is determined by the Young tableau [31]:

$$1s^{-1}\,1p^4\,[31]\,{}^{33}L : {}^{42}L; \tag{24a}$$

$$1s^{-1}\,1p^4\,[31]\,{}^{33}L : {}^{44}L; \tag{24b}$$

$$1s^{-1}\,1p^4\,[31]\,{}^{31}L : {}^{42}L. \tag{24c}$$

The [4] symmetry in the four-nucleon system is associ-

ated only with isospin $T = 0$. Therefore, the $1s^{-1}1p^4[4]$ configurations are realized in the system with isospin $T = \frac{1}{2}$ and cannot be manifested in the (π, γ) reaction.

In the system of four p nucleons with Young tableau [31] the orbital angular momenta $L = 1$, 2, and 3 can be realized. Spin-dipole transitions are associated with only the first two angular momenta because the orbital angular momentum of ^{7}Li in the ground state is $L = 1$: $|1s^4 1p^3[3]^{22}\mathrm{P}\rangle$, and the operator $[\sigma \otimes Y_1]$ cannot couple orbital angular momenta differing by more than one unit. States whose total angular momentum does not exceed $J_f = 5/2$ correspond to the configurations (24a) and (24c). It is only in the configuration (24b) that total angular momentum $J_f = J_i + 2 = 7/2$ is realized:

$$|1s^{-1},\ 1p^4\ [31]\ ^{33}D : {}^{44}D_{7/2}\rangle. \qquad (25)$$

The maximum in the region of γ energies around $E_\gamma = 120$ MeV corresponds to excitation of valence nucleons with predominant formation of the configurations

$$|1p^2\ [2]\ ^{31}S,\ 1d : {}^{42}D_J\rangle; \qquad (26a)$$

$$|1p^2\ [2]\ ^{31}D,\ 1d : {}^{42}L_J\rangle, \qquad (26b)$$

where $L = 0$, 1, and 2. In such configurations, the total angular momentum $J_f = J_i + 2 = 7/2$ is again not realized.

Calculation of the ^{7}Li(π, γ) reaction with the standard set of parameters leads to the appearance of a sharp peak at low ^{7}He excitation energies. As follows from the calculation, this peak corresponds to a resonance with $J_f^\pi = 5/2^+$ formed as a result of a $1p_{3/2} \to 1d_{5/2}$ transition. The theoretically obtained position of the maximum is shifted to lower energies by 4 MeV compared with the observed position. Calculation with the CK+ MK parameters (see Fig. 7b) leads to the necessary shift of the curve to higher energies, leaving practically unchanged the structure and the quantum numbers of the resonance. A similar effect was obtained in the calculation of the photoabsorption curve.[5]

As a result of electron scattering by ^{7}Li, states with isospin $T_f = T_i$ and also $T_f = T_i + 1$ larger by unity are excited. As follows from the calculations, the intensities of the two branches are almost the same. Therefore, the resulting excitation spectrum of ^{7}Li in the (e, e') reaction is complicated. The (π, γ) reaction makes it possible to cut out the $T_f = T_i$ branch and thus simplify the excitation curve.

The ^{9}Be *Nucleus.* The calculated excitation spectrum of the ^{9}Be nucleus in the (π, γ) (Fig. 8a), (e, e'), and photodisintegration reactions is fairly smooth. Since in this nucleus there are not such strong suppressions of the configurations as there are in ^{6}Li and ^{7}Li, the $\Delta J = 2$ transitions are fairly strong. As a result, the $M2$ resonance (see Fig. 7 in Ref. 61) is manifested much more clearly than in the two preceding nuclei. The nucleons of the valence $1p$ shell in ^{9}Be have the main strength of the transitions in the (π, γ) and photonuclear reactions and for electromagnetic $M2$ transitions. Blocking affects the $1s \to 1p$ transitions in the listed processes, and they are not so strong. Nucleons of the $1s$ shell manifest themselves clearly only in $E1$ excitations

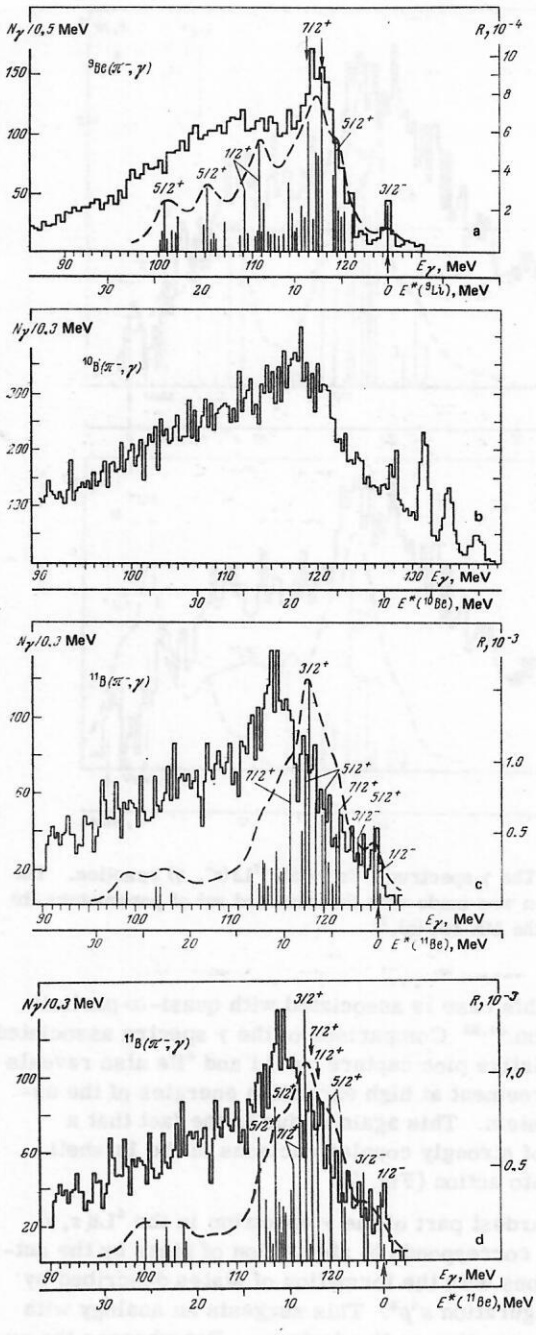

FIG. 8. The γ spectra of radiative pion capture: a) the ^{9}Be nucleus,[53] calculation in the standard variant; b) the ^{10}B nucleus[41]; c) the ^{11}B nucleus,[53] calculation in the standard variant; d) the same nucleus but calculated in the MK variant.

of transverse type. We have already explained the reason for this.

Since the $1s$ nucleons do not play such an appreciable part in the (π, γ) reaction in ^{9}Be, the entire excitation curve of the nucleus is shifted to lower energies (see Fig. 8), in contrast to the curves for the Li isotopes. It can be considered that overall the agreement between the theory and experiment for both the ^{9}Be(π, γ) reaction and photoabsorption is fairly good.

The ^{10}B *Nucleus.* In the γ spectra of radiative pion capture by the ^{10}B nucleus maxima are observed only in

the hardest part (see Fig. 8b). These are $M1$ and $M3$ transitions. In the energy region in which the $M2$ transitions must be localized and higher, there is almost no structure in the spectrum. The absence of structure is most probably due to the fact that the number of possible transitions is large and their superposition leads to smoothing of the resulting spectrum. A large number of states arises because the spin of the ground state of the ^{10}B nucleus is large: $J_i = 3$. Therefore, the response of the nucleus is associated with the excitation of states whose spin may reach five units. Unfortunately, a detailed theoretical analysis of the excitation of this nucleus has not yet been made.

The ^{11}B Nucleus. In the ^{11}B(π,γ) reaction, essentially only one maximum has been found (see Fig. 8c), and its width is appreciably less than in the preceding nuclei ($A = 6$–10). There is a low probability of transition to the ^{11}Be ground state ($1/2^+$). The calculation with the standard set of parameters of the nuclear model (CK + COP) leads to a strong concentration of the $1p_{3/2} \rightarrow 1d_{5/2}$ and $1p_{3/2} \rightarrow 1d_{3/2}$ transitions. The peak is obtained 5 MeV below the experimental peak. The situation is similar in ^{7}Li. We note that the Young tableaux of the ground-state wave functions of ^{7}Li and ^{11}B are almost identical ([3] and [43]). The photonuclear spectra are also not reproduced by the theory in such a variant. Replacement of the CK+ COP parameters by the CK+ MK parameters leads to a shift in the necessary direction of the positions of the maxima (see Fig. 8d) in both the (π,γ) and the photonuclear reaction, though agreement with experiment is still not achieved.

In both variants of the calculation, the principal maximum in the (π,γ) reaction is found to be associated with a resonance whose spin is $J_f = J_i = 3/2$. This is the only case in nuclei of the $1p$ shell when the theory associates the main maximum in the (π,γ) reaction with a $\Delta J = 0$ transition. In the photonuclear reactions, we have the usual situation, i.e., the spin of the main maximum is $J_f = J_i + 1 = 5/2$. It follows from what we have said that the ^{11}B nucleus is the most complicated case for the theory. In this connection, it appears desirable to make a more detailed investigation of it. In particular, inclusion of the decay characteristics discussed in Ref. 73 would make it possible to decompose the resonance into constitutent parts. The existence of such experimental information may significantly advance our understanding of the structure of the resonance states of this nucleus.

Carbon Isotopes (^{12}C, ^{13}C, *and* ^{14}C). For nuclei at the end of the $1p$ shell ($A = 12$–16) there are rather few data on inelastic electron scattering, photodisintegration, μ capture, etc. All the data can be described fairly well in the framework of the shell model. Similar agreement is observed for radiative pion capture. The results of investigation of electron scattering and radiative pion capture on ^{12}C has made it possible to assert with certainty that in this nucleus there is a concentration of $M2$-transition strengths.

Both in the γ spectrum of radiative pion capture by the nucleus ^{12}C and in the cross section of inelastic electron scattering it is possible to identify resonances

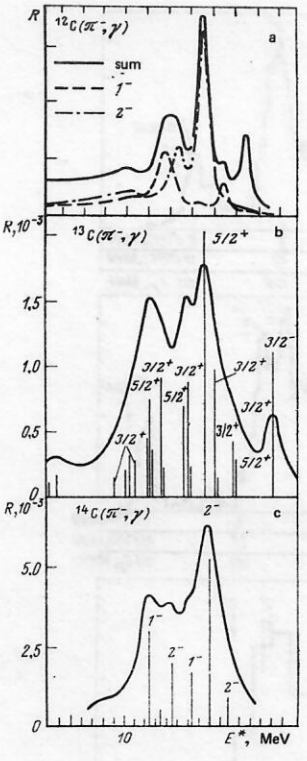

FIG. 9. Calculated γ spectra from radiative pion capture by carbon isotopes: a) the ^{12}C nucleus, calculations in accordance with the unified theory of nuclear reactions[7] with allowance for the continuum; b) the ^{13}C nucleus, calculation in the standard variant[18,72]; c) the ^{14}C nucleus, calculation in the standard variant.[19]

with spins $J = 1^+$, 1^-, and 2^- (Figs. 9 and 10). The highest intensity of the $M2$ transitions corresponds to the resonance whose excitation energy is $E^*(^{12}\text{C}) = 19.6$ MeV, which corresponds to $E^*(^{12}\text{B}) = 4.37$ MeV.[41] The resonance with quantum numbers $J^\pi = 1^-$ manifested in the (π,γ) reaction is interpreted as an analog of the photonuclear resonance $E^* = 22$ MeV.

Above the $J^\pi = 1^-$, $E^* = 22$ MeV resonance there is a region of ^{12}C excitation associated with transitions in which spin flip ($1p_{3/2} \rightarrow 1d_{3/2}$) occurs. In the ^{16}O nucleus, the theory predicted strong concentration of the strengths of such transitions in the (e,e') and (π,γ) reactions at the level $J^\pi = 1^-$, $E^* = 25$ MeV. However, in ^{12}C a significant maximum is observed neither in the measured nor in the calculated spectrum in this region of energies, although a certain concentration of the transition strengths can be traced. This is due to the fact that the spin-flip transitions in ^{12}C are strongly fragmented. This result is obtained in a theory which does not make the assumption that the $1p_{3/2}$ subshell in ^{12}C is closed.

Overall, the structure of the excitation spectrum of the ^{12}C nucleus in the (π,γ) reaction is well reproduced in the shell model (see Figs. 9 and 10) both with (Ref. 7) and without (Ref. 8) allowance for the continuum.

The ^{13}C nucleus has also been fairly well studied. There are detailed calculations of the total and partial photonucleon spectra.[5] They agree with the observed

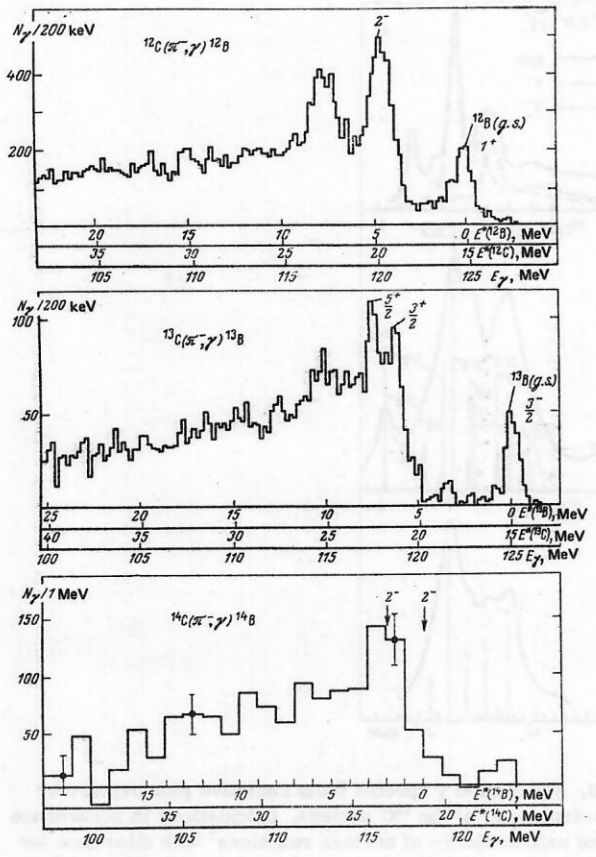

FIG. 10. Measured γ spectra for radiative pion capture by carbon isotopes: ^{12}C (Ref. 22), ^{13}C (Ref. 23), and ^{14}C (Ref. 17). The energy scales are shifted to achieve coincidence of the positions of the main maximum in all nuclei.

spectra.[74] There are experimental data[55] on electron scattering through large angles (145.7°). The theory reproduces the structure of the excitation spectrum of the nucleus.[72] Since the theory basically explains a large set of experimental data, the (π,γ) reaction should not be an exception. Indeed, subsequent measurements of the γ spectrum of the (π,γ) reaction on ^{13}C confirmed the predictions of the theory.

As follows from the calculations of Refs. 60 and 61, the transitions in the $^{13}C(\pi,\gamma)$ reaction are concentrated in a fairly narrow energy region. The ground-state spin of the ^{13}C nucleus is $1/2^-$. Therefore, the $M2$ resonance is split with respect to the spin ($J_f^\pi = 5/2^+$ and $3/2^+$). The strength of the $M2$ transitions is concentrated (see Refs. 18, 60, 61, and 72) in the resonances $J^\pi T = 5/2^+3/2$, $E^*(^{13}B) = 6.4$ MeV and $J^\pi T = 3/2^+3/2$, $E^*(^{13}B) = 5.5$ MeV,

TABLE IV. Partial γ yield in the $^{13}C(\pi,\gamma)$ reaction with excitation of positive-parity states.

E_γ	Experiment[23]			Theory[24]		
	E^* (^{13}C), MeV	E^* (^{13}B), MeV	R, 10^{-4}	R, 10^{-4}	J^π	E^* (^{13}B), MeV
121.5	18.6	3.5	0.96±0.4	8.1	3/2⁺, 5/2⁺	3.5
119.6	—	—	—	—	3/2⁺	
118.5	21.6	6.5	8.63±1.7	11.7	5/2⁺	5.5
117.4	22.7	7.6	10.23±1.8	24.5	5/2⁺, 3/2⁺	6.4
114.8	25.3	10.2	17.35±3.7	38.5	5/2⁺, 3/2⁺	8—11.6

TABLE V. Contributions of the main configurations to the wave functions of a number of resonances of the ^{13}B nucleus (in %).

Component of wave function	J^π; E (^{13}B), MeV		
	5/2⁺; (6.4)	3/2⁺; (5.5)	5/2⁺; (3.9)
$p_{3/2}^{-1}p_{1/2}d_{5/2}$	44	17	37
$p_{3/2}^{-1}p_{1/2}2s_{1/2}$	16	37	17

and also in the energy region $E^*(^{13}B) \approx 10$ MeV, where there are several states with $J^\pi = 3/2^+$ and $5/2^+$ (see Figs. 9 and 10 and Table IV). In the (π,γ) reaction, resonances with $E^* = 6.4$ and 5.5 MeV can be identified fairly clearly. The wave functions of these resonances contain the two large components

$$1p_{3/2}^{-1}1p_{1/2}^{1}1d_{5/2} \qquad (27a)$$

$$1p_{3/2}^{-1}1p_{1/2}^{1}2s_{1/2}. \qquad (27b)$$

The weights of these components in the wave function are given in Table V.

Table V also gives the wave-function structure of the level $J^\pi T = 5/2^+3/2$, $E^* = 3.9$ MeV, which, as can be clearly seen, is the spin–orbit partner of the level with $E^* = 5.5$ MeV. However, as follows from the analysis of the (π,γ) reaction, its excitation intensity is low.

Although the agreement between theory and experiment for ^{13}C is fairly good, it is important to make a more detailed investigation of the $^{13}C(e,e')$ reaction with high resolution. The results of such an investigation could establish the quantum numbers of the states that form the resonance.

The concentration of the $M2$- and $E1t$-transition strengths in the ^{14}C nucleus in the (π,γ) reaction and in electron scattering with small momentum transfer is fairly strong.[19] The gross structure of the excitation spectrum hardly depends on the parameters of the nuclear model. The strongest transitions are given in Table VI. As follows from the theory, the strength of the $M2$ transitions in both the (π,γ) and the (e,e') reaction is concentrated at the level $J^\pi T = 2^-2_2$ with excitation energy $E^*(^{14}B) = 1.8$ MeV, i.e., $E^*(^{14}C) = 24$ MeV. The $E1t$-transition strength is concentrated at a level 5 MeV higher. Preliminary experimental data on the $^{14}C(\pi,\gamma)$ reaction (see Fig. 10)[19] confirm the theoretical predictions. However, the γ yield is much lower than expected.

The $M2$ transition to the ground state ($J^\pi T = 2^-2_1$) of ^{14}B in the (π,γ) reaction and its analog in the ^{14}C nu-

TABLE VI. Strong transitions in $^{14}C(e,e')$ and $^{14}C(\pi,\gamma)$ reactions with excitation of resonances with isospin in $T=2$. The results in the MK variant are given in brackets.

J^π	E^* (^{14}C), MeV	E^* (^{14}B), MeV	E^* (^{14}B), MeV	$\frac{d\sigma}{d\Omega}$, 10^{-6} F²/sr	R, 10^{-4}
	Theory		Experiment		
1⁻	25.9	3.4 (4,8)	—	0	1.6 (0.5)
	29.3	6.8 (7,1)		2.3	2.7 (3.6)
2⁻	22.8	0.4 (0)	0	0.4	0.9 (0)
	24.2	1.8 (1,9)	1.82	1.7	5.3 (6.4)
	27.4	5.0 (5,1)		0.3	1.9 (2.0)

cleus in the case of electron scattering are weak. Its probability is sensitive to the parameters of the nuclear model. We believe it is important to continue the investigation of the $^{14}C(e,e')$ reaction at large angles. The earlier measurements[75] were unfortunately restricted to low excitation energies.

We now turn to a comparison of the excitation spectra of the nuclei of the carbon isotopes. In all the nuclei, the structure of the main maximum of the $M2$ transition for ^{12}B ($J^\pi = 2^-$, $E^* = 4.37$ MeV), ^{13}B ($J = 5/2^+$, $E^* = 6.4$ MeV), and ^{14}B ($J^- = 2^-$, $E^* = 1.8$ MeV) is due to the component $1p_{3/2}^{-1}1p_{1/2}^{A-12}1d_{5/2}$. The coincidence of the main maxima in the three nuclei (see Figs. 9 and 10) clearly demonstrates the generality of the nuclear response in these three isotopes. Next to the main maximum at higher excitation energies of the nucleus there are less clearly expressed maxima, which are associated with the states that form the dipole resonance in the photonuclear reactions, and somewhat higher there is a dipole resonance with spin flip ($E1t$).

We now arrange the excitation spectra of the nuclei in the (π,γ) and (e,e') reactions to achieve coincidence of the positions of the strong peaks corresponding to the $M2$ transitions (Figs. 11 and 12). In the case of the $T_>$ $M2$ transitions, the theory predicts a two-hump excitation curve for electron scattering. We recall that in ^{16}O such a picture was observed. In the (π,γ) reaction, the excitation curve has a similar structure, and it is expressed even more clearly because of the enhancement of the intensity of the second (situated at higher nuclear excitation energy) hump. This enhancement is due to the inclusion of transitions that in the (e,e') reaction form the $E1t$ resonance. The reason for the appearance of the two humps is the spin–orbit splitting. The low-energy hump is associated mainly with the $1p_{3/2} \to 1d_{5/2}$ transition, and the upper one with the $2p_{3/2} \to 1d_{3/2}$ transition. In the measured spectra of the (π,γ) transitions, the presence of two humps can also be established.

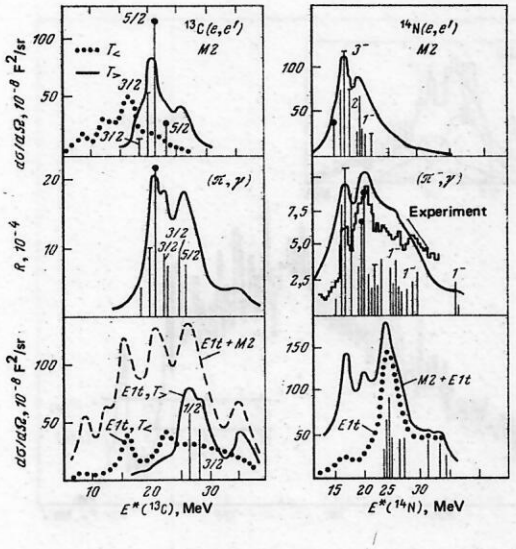

FIG. 11. Comparison of calculated spectra of spin excitations of the ^{13}C and ^{14}N nuclei for inelastic electron scattering and radiative pion capture with separation of the multipoles.

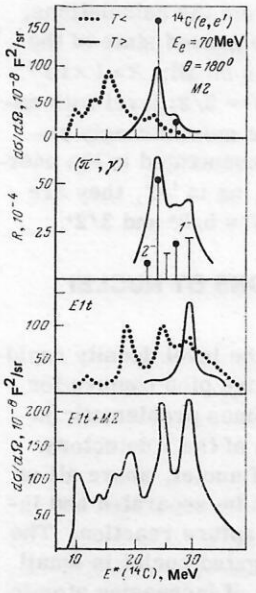

FIG. 12. Comparison of calculated spectra of spin excitations of the ^{14}C nucleus for inelastic electron scattering and radiative pion capture with separation of the multipoles.

The ^{14}N Nucleus. The excitation curve of ^{14}N was found to be insensitive to the choice of the parameters of the nuclear model. Use of the interaction proposed in Ref. 6, or the standard CK+ COP interaction, or the CK+ MK interaction leads to almost exactly the same shape of the excitation spectrum of the nucleus. Figure 13 shows the γ spectrum of radiative pion capture by the ^{14}N nucleus measured at SIN,[48] and also the results of calculation in the standard approach.[18] The transition strength is concentrated at the $J^\pi = 3^-$ level, which takes an appreciable fraction of the total intensity. The most intense peak with $J^\pi = 2^-$, situated near the peak with $J^\pi = 3^-$, is the analog of the dipole resonance in the case of γ absorption.

In the calculated and measured excitation spectra of ^{14}N in the (π,γ) reaction one can identify the two humps discussed above (see Fig. 11). With regard to electron scattering, there are as yet only provisional data[76] on $M2$ transitions.

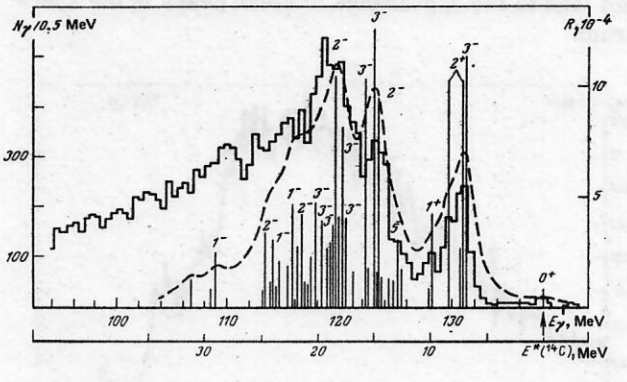

FIG. 13. The γ spectrum in the $^{14}N(\pi,\gamma)$ reaction. The histogram is taken from Ref. 47 and the calculation is in the standard variant.[18]

The ^{15}N *Nucleus*. As follows from the calculations, the probability of excitation of the ground state of the ^{15}C nucleus in the (π,γ) reaction is small: $R\approx 1\times10^{-4}$. Among the ^{15}C bound states, the $J^\pi = 5/2^+_1$ level with energy $E^*(^{15}\text{C}) = 0.75$ MeV is the one most strongly excited. The $M2$ transitions are concentrated in the energy region from 8 to 15 MeV, and, as in ^{13}C, they are distributed over states with spin $J^\pi = 5/2^+$ and $3/2^+$.

2. RADIATIVE CAPTURE OF PIONS BY NUCLEI HEAVIER THAN OXYGEN

In nuclei heavier than oxygen, the level density rapidly increases and the use of radiative pion capture for spectroscopic investigations becomes problematic in view of the insufficient resolution of the γ detectors. There are, however, examples of nuclei, above all in the $2s-1d$ shell, whose states can be separated and investigated in the radiative-pion-capture reaction. The number of experimentally investigated nuclei is small. In this section, we give, in order of increasing atomic number A, the nuclei for which there are experimental data on radiative pion capture.

The ^{18}O *Nucleus*. This nucleus was partly discussed in the review of Ref. 1. The two neutrons in the $2s-1d$ shell do not participate directly in the capture process. Therefore, the γ spectrum in the $^{18}\text{O}(\pi,\gamma)$ reaction recalls the spectrum in ^{16}O. However, the presence of the two neutrons in the valence shell leads to blocking of a number of states of the final nucleus. As a result, there is a regrouping of the transitions. In ^{16}O, a clear grouping of the strengths of the spin-quadrupole transitions is not observed. In ^{18}O, a small maximum can be seen in the region of localization of these transitions. This clear grouping of the transition strengths in ^{18}O was interpreted in Ref. 77 as indicating the existence of concentration of the spin–quadrupole excitations in this nucleus.

The ^{19}F *Nucleus*. Because of the proton present in the $2s$ or $1d$ shell, transitions to low-lying bound states of ^{19}O are possible. However, these transitions have low intensity, since the structures of the low-lying ^{19}O levels and of the ^{19}F ground state (Fig. 14 and Table VII) differ rather strongly.[78] In muon capture by the ^{19}F nucleus, there is a similar situation.[51,79] With regard to pion capture by protons of the $1p$ shell, it does not lead to the appearance of clear peaks in the spectrum.

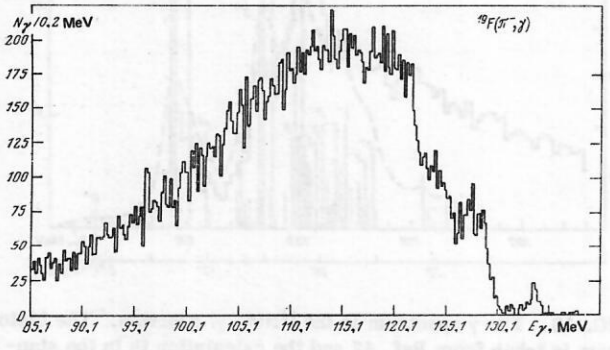

FIG. 14. The γ spectrum for the $^{19}\text{F}(\pi,\gamma)$ reaction.[23]

TABLE VII. The γ yield in the $^{19}\text{F}(\pi^-,\gamma)$ reaction (experiment)[23] and the rate of muon capture by the ^{19}F nucleus (theory).[51,79]

E_γ, MeV	E^* (^{19}F), MeV	E^* (^{19}O), MeV	J^π	R_γ, 10^{-4}	Λ_μ, sec^{-1}
133.6	(7.6)	0.0	$5/2^+$	1.3±0.3	—
133.5	(7.7)	0.097	$3/2^+$		1000
132.1	(9.1)	1.468	$1/2^+$		190
131.2	(10.0)	2.370	$3/2^+$	<0.5	210
130.4	(10.9)	3.237	$1/2^+$		200
128.6	(11.5)	3,9	$3/2^-$	4.5±0.9	
127.2	(12.2)	4,6	$3/2^-$	4.8±1.0	—
125.6	(13.9)	6,3	$7/2^-$	3.2±0.75	
124.8	(18.6)	11,0	$5/2^-$	2.7±0.6	
Smooth background				223±46	
Total yield				240±48	

The ^{20}Ne *Nucleus*. The γ spectrum for the radiative capture of pions by the ^{20}Ne nucleus obtained recently at Los Alamos is shown in Fig. 15.[23] A clear resonance structure is observed in the spectrum at low excitation energies; a fairly strong $M1$ peak is observed in this region in electron scattering.[80] The result of the analysis of the experimental γ spectrum is given in Table VIII. A more detailed examination shows that the radiative-pion-capture peak is formed by two $J^\pi = 2^-$ states, and the contribution of the $J^\pi = 1^+$ level is small. A qualitative and quantitative explanation of this will be given in Sec. 3. Here we mention as result of the calculation that the $J^\pi = 2^-$ states play an important part in the (e,e') reaction on ^{20}Ne.[81] In particular, the second peak in the spectrum at excitation energy $E^* = 6.1$ MeV of the final nucleus can be interpreted as a manifestation of a $J^\pi = 2^-$ state. The observed strength of the transitions in the (π,γ) reaction can be used for quantitative determination of the contribution of correlations in the ground state of the target nucleus. Such an approach was first realized in analysis of $M2$ transitions

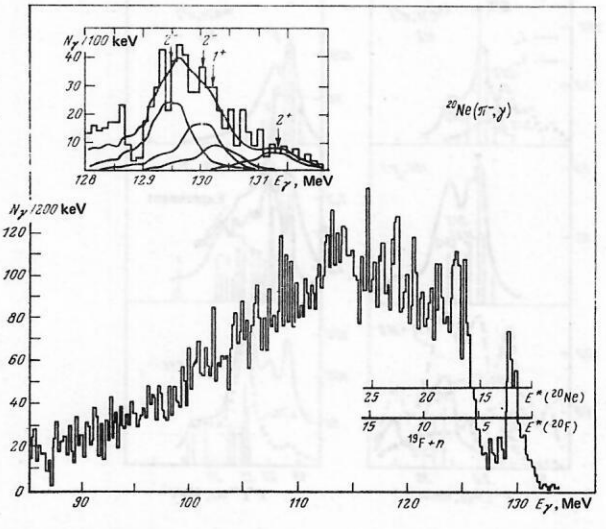

FIG. 15. The γ spectrum for the $^{20}\text{Ne}(\pi,\gamma)$ reaction from Ref. 38. The inset shows on an enlarged scale the contributions of the four levels that form the peak near $E_\gamma = 130$ MeV.

TABLE VIII. Results of analysis of the γ spectrum for the $^{20}Ne(\pi^-, \gamma)$ reaction.[38]

E_γ, MeV	E^* (^{20}Ne), MeV	E^* (^{20}F), MeV	R_γ, 10^{-4}	R_γ/R_γ^{tot}, %	J^π
131.3	10.2	0.0	0.7±0.3	0.42	2^+
130.2	11.3	1.1	0.9±0.5	0.57	1^+
130.0	11.5	1.3	1.7±0.6	1.07	2^-
129.5	12.0	1.8	2.6±0.3	1.61	2^-
125.2	16.3	6.1	15.3±3.0	9.55	—
114.2	27.3	17.1	14.8±1.7	3.0	—
Smooth background			134±22	83.0	
Total yield			160±24	100	

in inelastic electron scattering.[80] However, the analysis gives γ yields in the (π, γ) reaction that are too high.

The ^{28}Si *Nucleus*. Experimentally, the ^{28}Si nucleus is an interesting object. The decay threshold of the ^{28}Al nucleus formed through the $^{27}Al + n$ channel is high (7.7 MeV). Therefore, in the hardest part of the γ spectrum there is a background-free window of width almost 8 MeV. Data on inelastic electron scattering revealed[82] in this region several levels excited as a result of $M1$ and $M2$ transitions. Analysis of the results on the basis of the shell model made it possible to obtain a fairly accurate picture of the correlations that determine the structure of the wave function of these states.

The experimental γ spectrum in the $^{28}Si(\pi, \gamma)$ reaction is shown in Fig. 16. Analysis reveals four states with quantum numbers $J^\pi = 1^+$ and three with $J^\pi = 2^-$ and permits determination of the γ yields corresponding to them. The calculation reflects qualitatively the energy dependence of the γ yields. The energy positions of the levels agree with the observed positions only approximately. Simultaneous analysis of the $^{28}Si(e, e')$ and $^{28}Si(\pi, \gamma)$ reactions makes it possible to separate spin and orbital components of the $M1$-transition matrix element in the same way as was done in ^{20}Ne. Such analysis in the framework of a microscopic approach is one of the elements in the verification of the wave functions obtained on the basis of the shell model.[83] The final aim of such calculations is to determine the spin-dependent part of the effective nucleon interaction in nuclei.

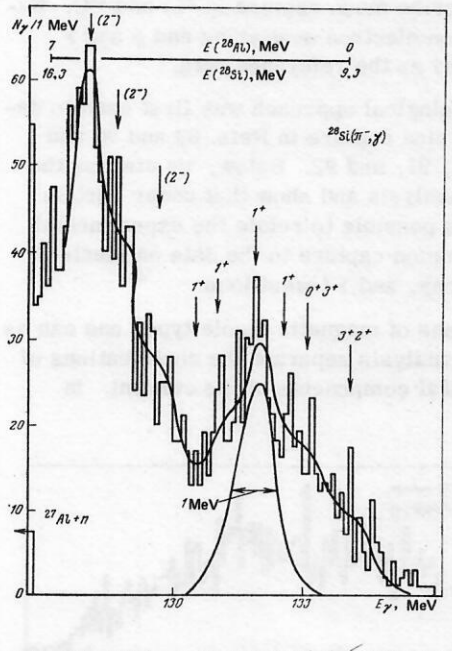

FIG. 16. High-energy part of the γ spectrum in the $^{28}Si(\pi, \gamma)^{28}Al$ reaction.[53] The events below the $^{28}Al \to ^{27}Al + n$ decay threshold were eliminated when the experimental data were analyzed on the basis of the pole model.

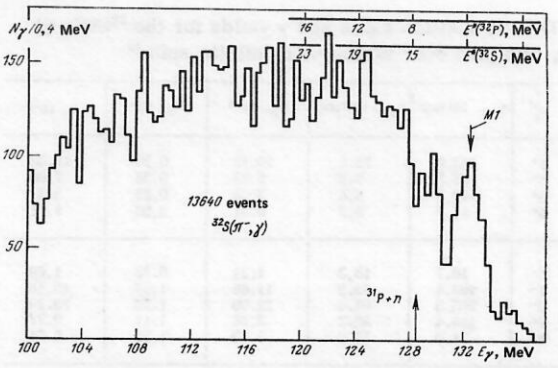

FIG. 17. The γ spectrum in the $^{32}S(\pi, \gamma)$ reaction.[84]

The ^{32}S *Nucleus*. In contrast to the ^{28}Si nucleus, a peak is observed[84] in the γ spectrum of radiative pion capture in ^{32}S only in the region of the hardest γ rays. It is associated with transitions of the valence nucleons within one shell (Fig. 17). At lower γ energies there is a strong overlapping of the spin-dipole, spin-quadrupole, and spin-octupole excitations. Such an interpretation is based on a semiquantitative analysis[85] based on single-particle estimates of the transitions in ^{32}S. We recall that in ^{16}O the spin-quadrupole transitions are responsible for the γ yield in less than 50% of the cases. In ^{32}S, they become predominant (Table IX), and the spin-octupole transitions associated with the operator $[\sigma \otimes Y_3]$ give the next largest contribution. All this is a consequence of the increasing importance of pion capture from the $3d$ orbit (in the calculation, it was assumed that capture from this orbit takes place in 10% of the cases). The resulting spectrum is formed as a result of the superposition of a large number of transitions, and the structure is completely lost.

Medium and heavy nuclei

Radiative capture of pions has also been experimentally investigated for the four heavier nuclei ^{40}Ca, ^{90}Zr, ^{208}Pb, and ^{209}Bi. The corresponding γ spectra are given in Figs. 18–21. For ^{40}Ca and ^{90}Zr one notes a certain structure in the high-energy part of the γ spectrum. However, there is as yet no quantitative analysis of the corresponding transition intensities.

In Refs. 2 and 86 there is a fairly detailed discussion of the structure of the γ spectrum in ^{209}Bi. However, it should be borne in mind that the two experiments made for this nucleus gave contradictory results.

Following the theoretical analysis made in Ref. 87 for capture by the ^{208}Pb nucleus, we can readily establish

TABLE IX. Transition rates and γ yields for the $^{32}S(\pi^-, \gamma)$ reaction, summed over states with definite spin.[85]

$N\hbar\omega$	J_f^π	Λ_{2p}, 10^{13}sec^{-1}	Λ_{3d}, 10^{10}sec^{-1}	R_p, 10^{-4}	R_d, 10^{-4}	R, 10^{-4}
$0\hbar\omega$	1^+	143.0	22.6	10.73	0.59	11.32
	2^+	91.3	9.0	6.83	0.23	7.06
	3^+	42.7	8.6	3.24	0.23	3.47
	4^+	11.7	8.3	0.91	0.20	1.11
$1\hbar\omega$	0^-	16.7	13.3	1.24	0.36	1.60
	1^-	155.4	55.5	11.66	1.47	13.13
	2^-	295.3	64.4	22.09	1.70	23.79
	3^-	115.4	42.2	8.66	1.11	9.77
	4^-	71.0	52.2	5.33	1.38	6.71
$2\hbar\omega$	1^+	128.6	25.5	9.66	0.68	10.34
	2^+	336.0	48.9	25.20	1.29	26.49
	3^+	257.2	71.7	19.31	1.90	21.21
	4^+	24.5	30.0	1.83	0.79	2.62
	5^+	17.4	28.8	1.33	0.75	2.08
$3\hbar\omega$	1^-	69.2	5.4	5.19	0.14	5.33
	2^-	119.8	23.6	8.98	0.62	9.60
	3^-	91.0	59.1	6.82	1.56	8.38
	4^-	47.9	45.8	3.59	1.21	4.80
$0\hbar\omega$	ΣJ_f^π	288.7	48.5	21.71	1.25	22.96
$1\hbar\omega$	ΣJ_f^π	653.8	277.6	48.98	6.02	55.00
$2\hbar\omega$	ΣJ_f^π	763.7	204.9	57.33	5.41	62.74
$3\hbar\omega$	ΣJ_f^π	327.9	133.9	24.59	3.53	28.12
Total yield		2034.1	614.9	152.61	16.21	168.8

the reason for the disappearance of structure in the γ spectrum. Capture takes place mainly from a high ($l_\pi \approx 3$) mesoatomic orbit, and $kR \approx 5$ (the energy carried away by the γ ray, multiplied by the radius of the nucleus). Therefore, in the final nucleus levels whose spins can take values up to $J = 8$ can be excited. The superposition of all the transitions leads to the smooth spectrum. We have already noted a similar effect in the ^{32}S nucleus, and it is also noted in analysis of the γ spectrum of radiative pion capture by ^{40}Ca in the second of the papers quoted in Ref. 84. Thus, the (π^-, γ) reaction on heavy nuclei does not possess the selectivity with respect to definite excitation modes that there is in the case of light nuclei.

3. PHENOMENOLOGICAL APPROACH TO THE DESCRIPTION OF PARTIAL TRANSITIONS IN LIGHT NUCLEI

The characteristics of nuclear transitions discussed above were calculated on the basis of definite nuclear

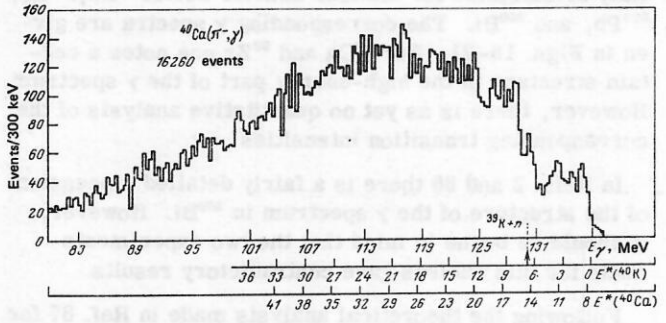

FIG. 18. The γ spectrum for the $^{40}Ca(\pi^-, \gamma)$ reaction.[84]

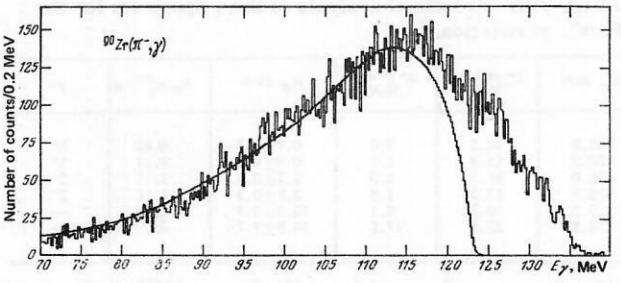

FIG. 19. The γ spectrum for the $^{90}Zr(\pi, \gamma)$ reaction.[23] The histogram gives the results of the measurements, the curve the result of fitting on the basis of the pole model.

wave functions constructed in definite variants of the shell model. This approach revealed certain general regularities of radiative pion capture for a wide region of nuclei. At the same time, the connection of radiative pion capture with other processes such as muon capture and electron scattering was revealed. In the establishment of the connection, the nuclear wave functions play the part of intermediaries. The use of model wave functions to calculate nuclear matrix elements generally introduces an uncertainty that is difficult to control. Therefore, is it possible to do without wave functions altogether or to reduce the part they play to a minimum?

The problem is solved from this point of view in the so-called phenomenological approach. However, it is not as a rule possible to do without wave functions entirely. The part played by the models reduces in this case to their being employed to identify the most important parts of the matrix elements, which are then not calculated but taken from other experiments. In particular, such an approach was already used in Refs. 37 and 88 to describe muon capture in ^6Li and ^{12}C. Experimental data on electron scattering and β and γ transitions served as the reference data.

The phenomenological approach was first used to describe radiative pion capture in Refs. 89 and 90 and later in Refs. 53, 91, and 92. Below, we discuss the results of such analysis and show that under certain assumptions it is possible to relate the experimental data on radiative pion capture to the data on electron scattering, β decay, and γ transitions.

For γ transitions of magnetic dipole type, one can as a result of such analysis separate the contributions of the spin and orbital components of the current. In

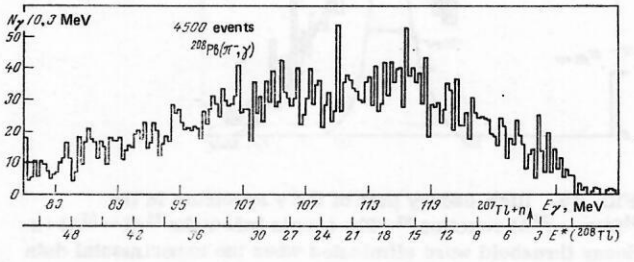

FIG. 20. The γ spectrum for the $^{208}Pb(\pi, \gamma)$ reaction.[86]

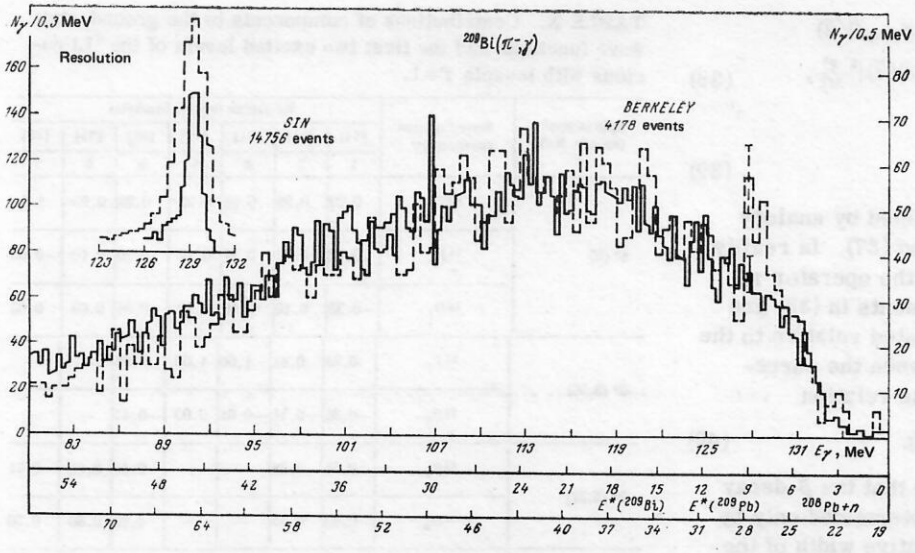

FIG. 21. The γ spectrum for the ^{209}Bi(π, γ) reaction.[86]

other cases, in particular for a pure magnetic octupole ($M3$) γ transition and the corresponding (π, γ) transition in nuclei of the $1p$ shell (when only one matrix element is nonzero), the connection between the characteristics of these processes makes it possible to judge the consistency of the measured quantities. When the number of basis configurations in the wave functions is small, as is the case in ^{6}Li, the amplitudes of the components can be extracted directly from the experimental data.

In the phenomenological analysis of radiative pion capture by nuclei, a number of simplifications are generally made[22,53,48]:

1. The wave function of a pion in the $1s$ orbit is expressed as the product of a hydrogenlike function (in the field of a point charge) and a correction factor C_{1s} (see Eq. (40) in Ref. 1). Since the pion function changes slowly in the volume of the nucleus, it is taken in front of the integral sign in the matrix element and replaced by a constant, for example,

$$|\Phi^\pi_{1s}(0)|^2 = 4C_{1s}a_\pi^{-3}, \tag{28}$$

where a_π is the Bohr radius:

$$a_\pi = (1+m_\pi/M_A)/\alpha Z m_\pi. \tag{29}$$

2. The wave function for a pion in the $2p$ orbit is approximated by the expression

$$|\Phi^\pi_{2p}|^2 = C_{2p}r^2/(24a_\pi^5), \tag{30}$$

where C_{2p} is the correction factor for the $2p$ orbit.

3. The radial integrals in the transition matrix elements were calculated using harmonic-oscillator functions. The oscillator parameter r_0 is determined using electron scattering data.

As a result of these simplifications, the operators $O_A(J;L,l)$ and $O_B(J;L,l)$ describing the radiative pion capture are reduced to sums of operators of two types: $\tau_-[\sigma\otimes Y_L]_J$ and $\tau_- Y_L$, where $\tau_-|p\rangle = |n\rangle$. The second type arises from the term of the Hamiltonian proportional to the constant D. All the remaining terms lead to operators of the first type.

If the pions are captured from the $1s$ orbit, it is sufficient to make a restriction to the terms of the Hamiltonian proportional to the constant A.[1,7,8,48] Then

$$\begin{aligned} O_A(J=L;\,L,\,0) &= [A(4C_{1s}a_\pi^{-3})^{1/2}/(4\pi)^{1/2}] \\ &\times\{\sqrt{L/(2L+1)}\, j_{L+1}(qr)\,\tau_-[\sigma\otimes Y_{L+1}]_L \\ &-\sqrt{(L+1)/(2L+1)}\, j_{L-1}(qr)\,\tau_-[\sigma\otimes Y_{L-1}]_L\}; \end{aligned} \tag{31}$$

$$O_B(J=L;\,L,\,0) = -[A(4C_{1s}a_\pi^{-3})^{1/2}/(4\pi)^{1/2}]\, j_L(qr)\,\tau_-[\sigma\otimes Y_L]_L. \tag{32}$$

We denote by F_l the radial integrals

$$F_l = \exp\left(\frac{r_0^2q^2}{4(N+Z)}\right)\int_0^\infty R^2_{1p}(r)\, j_l(qr)\, r^2\, dr \begin{cases} 1, \text{ if } l \text{ is even}, \\ r, \text{ if } l \text{ is odd}, \end{cases} \tag{33}$$

where r_0 is the oscillator parameter, q is the momentum transfer, and $N+Z$ is the number of nucleons.

To be specific, we now consider a $J^\pi = 1^+ \to 0^+$ transition. The matrix element of radiative pion capture for such a transition takes the form

$$\begin{aligned} 1s:\ &|\langle 0^+\|O_A(1;1,0)\|1^+\rangle|^2 \\ &= \frac{A^2a_\pi^{-3}C_{1s}}{\pi}\left|\sqrt{\tfrac{1}{3}}F_2R_{21} - \sqrt{\tfrac{2}{3}}F_0R_{01}\right|^2; \end{aligned} \tag{34}$$

$$\begin{aligned} 2p:\ &\left|\langle 0^+\|O_B\left(1;\tfrac{2}{1},0\right)\|1^+\rangle\right|^2 \\ &= [a_\pi^{-5}C_{2p}/(32\pi)]\left|\sqrt{\tfrac{1}{3}}[\pm AF_1 + q(\pm B+C)F_0]R_{01}\right. \\ &+\left.\sqrt{\tfrac{1}{6}}\{-A/10[(7\pm5)F_3+(1\pm1)F_1]+q[\mp B+2C]F_2\}R_{21}\right|^2. \end{aligned} \tag{35}$$

As follows from (34) and (35), the rate of the (π,γ) transition between the states $J^\pi = 0^+$ and 1^+ is determined by two matrix elements:

$$R_{01} = \langle 0^+\|[\sigma\otimes Y_0]_1\tau_-\|1^+\rangle; \tag{36}$$

$$R_{21} = \langle 0^+\|[\sigma\otimes Y_2]_1\tau_-\|1^+\rangle. \tag{37}$$

The same matrix elements determine the form factor of the $M1$ transition for electron scattering. But besides them, the form factor contains matrix elements of the operator of the convection current[93]:

$$F_T^2 = \frac{2\pi}{Z^2}\frac{1}{2J_i+1}\left|\left[(g_p^l - g_n^l)/2\sqrt{3}\right]\left|(F_2 L_{21} - F_0 L_{01}/\sqrt{2})\right.\right.$$
$$\left.\left. + \left[(g_p^s - g_n^s)/8\right](-F_2 R_{21}/\sqrt{3} + \sqrt{2}F_0 R_{01}/\sqrt{3})\right|^2 \frac{q^2}{M_p^2}, \quad (38)$$

where

$$L_{LJ} = \langle f \| \tau_- [L \otimes Y_L]_J \| i \rangle. \quad (39)$$

The matrix element (39) is determined by analogy with the spin matrix elements (36) and (37). In reality, (38) contains the matrix elements of the operator τ_3. For convenience, all the matrix elements in (38) are expressed in isospin coordinates rotated relative to the initial coordinates through 90°. Between the corresponding matrix elements there is the relation

$$\langle f \| \tau_3 [\sigma \otimes Y_0]_1 \| i \rangle = (-1)^{J_f - J_i + 1} R_{01}/\sqrt{2}. \quad (40)$$

Without going into details, we note that the β-decay rate in the $J^\pi = 0^+ \to 1^+$ transition is determined only by the matrix element R_{01}, and the radiative width of the level is determined by the matrix elements L_{01} and R_{01}, since in the limit $q^2 \to 0$ the contribution of L_{21} and R_{21} vanishes.

A similar analysis can be made for transitions between states with other spins. We give corresponding examples later. The approach can be extended to nuclei of the $2s-1d$ shell, in which capture of pions from the $2p$ orbit is predominant.

The general scheme of the approach is as follows. From the experimental data on inelastic electron scattering at small momentum transfers q the sum of the matrix elements L_{01} and R_{01} is determined, and from the data at large q the sum of the matrix elements L_{21} and R_{21}. If a β transition takes place between the considered states, its rate determines the matrix element R_{01}. Then the remaining matrix element R_{21} is found from the radiative pion capture. If a β transition is not realized, then R_{01} is extracted from radiative-pion-capture data, and one must ignore the matrix element R_{21}, which is usually small.

We now discuss the results of the implementation of the phenomenological approach for definite transitions.

The ^{6}Li *Nucleus*. The most extensive experimental data are available on the transition from the ground state of ^{6}Li ($J = 1^+$, $T = 0$) to the excited $J^\pi T = 0^+1$ state with energy $E^* = 3.56$ MeV. The analog of this level in the ^{6}He nucleus is its ground state. This transition was already discussed in Ref. 2. However, at that time there were no experimental data on capture from the $1s$ state of the mesic atom. Therefore, we discuss this transition. Simultaneously, we discuss transitions to the level $J^\pi T = 2^+1$, $E^* = 5.37$ MeV of the ^{6}Li nucleus and its analog in ^{6}He, since more accurate data have been published on electron scattering[91,92] and radiative pion capture.[22,62]

Under the assumption that the $1s$ shell is closed, the wave functions of the listed states contain a small number of components, which makes it possible to determine the contribution of each of them by analyzing the characteristics of the transitions. Indeed, in the LS representation the functions can be expressed in the form of the expansions[44,91]

TABLE X. Contributions of components to the ground-state wave functions and the first two excited levels of the ^{6}Li nucleus with isospin $T = 1$.

Spin of level (energy, MeV)	Wave-function components	Reference (square brackets)						
		[14]	[91]	[91]	[96]	[92]	[95]	[95]
		1	2	3	4	5	6	7
1^+ (0)	$^{13}S_1$	0.99	0.92	0.92	0.92	0.98	0.99	1.0
	$^{11}P_1$	0.12	0.37	0.37	0.37	0.20	0.10	—0.08
	$^{13}D_1$	—0.33	0.10	0.10	0.10	0.04	0.03	0.03
0^+ (3.56)	$^{31}S_0$	0.93	0.84	1.00	1.00	0.88	—	—
	$^{33}P_0$	—0.36	—0.54	—0.01	0.03	—0.47	—	—
2^+ (5.37)	$^{33}P_2$	0.55	0.36	—	—	0.46	0.60	—0.71
	$^{31}D_2$	0.83	0.93	—	—	0.89	0.80	0.70

$$|1^+,\ T=0\rangle = \alpha\,|{}^{13}S_1\rangle + \beta\,|{}^{11}P_1\rangle + \gamma\,|{}^{13}D_1\rangle; \quad (41)$$

$$|0^+,\ T=1\rangle = a\,|{}^{31}S_0\rangle + b\,|{}^{33}P_0\rangle; \quad (42)$$

$$|2^+,\ T=1\rangle = c\,|{}^{33}P_2\rangle + d\,|{}^{31}D_2\rangle. \quad (43)$$

By virtue of the normalization condition, $a^2 + b^2 = c^2 + d^2 = \alpha^2 + \beta^2 + \gamma^2 = 1$. The four matrix elements R and L discussed above can be expressed in a definite manner in terms of the coefficients α, β, γ, etc. Thus, for transitions to the level $J^\pi = 0^+$

$$R_{01} = (\sqrt{6}\,\alpha a + \sqrt{2}\,\beta b)/\sqrt{4\pi} \approx 0.62; \quad (44)$$

$$R_{21} = (\sqrt{10}\,\beta b + 2\sqrt{6}\,\gamma a + 3\sqrt{3}\,\gamma b)/\sqrt{4\pi} \approx 0.04; \quad (45)$$

$$L_{01} = \sqrt{2}\,L_{21} = (-2\alpha b + 2\sqrt{3}\,\beta a + \sqrt{5}\,\gamma b)/\sqrt{4\pi} \approx 0.32. \quad (46)$$

The coefficients in the ground-state wave function of ^{6}Li are fixed by the data on the magnetic and quadrupole moments of the level. The function obtained in this manner differs from the function that is obtained in Ref. 14 and reproduces the positions of the levels only by the weight of the small components β and γ.

Inelastic electron scattering was analyzed with a view to finding the coefficients a and b in Refs. 91 and 94. The result of the analysis is not unique—there are two solutions. In one, the contribution of the P component is large, while in the other this component hardly appears. The two solutions are given in Tables X–XII. Also given there are the characteristics of various pro-

TABLE XI. Electromagnetic and weak transitions in the ^{6}Li and ^{6}He nuclei (the corresponding wave functions are given in Table X; references are indicated by square brackets).

№	μ, μ_N	Q, mb	ft, sec^{-1}	Γ_γ^0, eV		F_T^2 (q=0.68 10^{-3} F^{-1}),			Λ_μ, sec^{-1}
	1^+	1^+	0^+	0^+	2^+	0^+	2^+	$2^+/0^+$	0^+
1	0.87	1.34	725	8.41	0.36	1.68	0.45	0.27	
2	0.82	—0.80	822	8.14	0.27	1.65	0.45	0.28	1187
3	0.82	—0.80	765	8.15		1.74			1231
4	0.82	—0.80	779	7.96		1.70			
5	0.86	—0.66	780	8.17	0.27	1.66	0.47	0.28	
6	0.88	—0.83			0.22		0.46		
7	0.88	—0.83			0.07		0.47		
Experiment	0.82	—0.80 ±0.08	[39] 815	[91] 8.16 ±0.19		[91] 1.60 ±0.05	[92] 0.53 ±0.06	0.33 ±0.04	[96] 1600^{+300}_{-129}

TABLE XII. Characteristics of radiative pion capture by the ^{6}Li nucleus (the corresponding wave functions are given in Table X; references are indicated by square brackets).

№	Λ_γ^{1s}, 10^{15} sec^{-1}			Λ_γ^{2p}, 10^{10} sec^{-1}			$\alpha(^6\text{Li}\to{}^6\text{He})/\alpha(p\to n)$		
	0^+	2^+	$2^+/0^+$	0^+	2^+	$2^+/0^+$	0^+	2^+	$2^+/0^+$
1	1.60±0.04	0.48	0.30	5.0±0.5	4.0	0.80	0.110	0.041	0.37
2	1.38±0.03	0.53	0.38	4.3±0.5	4.2	0.98	0.094	0.046	0.49
3	1.62±0.04			4.5±0.5			0.113		
4	1.60±0.04			4.5±0.5			0.111		
5	1.47±0.04	0.54	0.37	4.5±0.5	4.3	0.95	0.101	0.046	0.46
6		0.45			3.6			0.039	
7		0.34			2.8			0.029	
		[48]						[97]	
Experiment	1.44±0.15	0.32 ±0.07	0.22 ±0.05	5.4±1.8	3.0 ±0.9	0.48 ±0.11	0.098 ±0.004	0.068 ±0.024	0.70 ±0.24
		0.46 ±0.08	0.32 ±0.05		4.0 ±1.2	0.58 ±0.11			

Note. The experimental values of $\Lambda_\gamma(2^+)$ are obtained after subtraction of the continuum contribution in the $^4\text{He}+nn$ channel (upper value) or $^5\text{He}+n$ channel (lower value).

cesses calculated with the two sets of coefficients. The oscillator parameter was taken to be $r_0 = 2.03$ F.

It follows from Table XII that only the set of coefficients corresponding to a large contribution of the P component can explain the pion-capture data. Note that the calculation made in Ref. 14 also leads to a large contribution of the P component. If the ^{6}Li ground state contains an appreciable P component, this will affect the cluster decay channel of the hypernucleus $^6_\Lambda$Li* formed in the (K^-,π^-) reaction at angle $\theta_\pi = 0°$. As a result of the decay $^6_\Lambda\text{Li}^* \to d + {}^4_\Lambda\text{He}^*$, excited $^4_\Lambda$He is formed in the final state and then emits a γ ray with energy 1.1 MeV.[98] The only quantity that cannot be reproduced in the phenomenological approach is the muon capture rate.[96]

We now discuss transitions to a $J^\pi = 2^+$ level. The wave function obtained in Ref. 92 by analyzing the experimental data on electron scattering also reproduces the results of the measurements of the (π,γ) reaction. At the same time, the wave function is close to the one obtained as a result of a model calculation.[14] The ratios of the γ yields in the (π,γ) reaction associated with the transitions to the $J^\pi = 0^+$ and 2^+ levels deviate in such an analysis from the measured values. It should be noted that a ratio of yields is determined much more accurately than the absolute values, especially in the case of pion capture from the $2p$ orbit. The theory gives for the ratio the value 0.95, whereas it follows from the experiment[22] that it is 0.48 ± 0.11 or 0.58 ± 0.11, depending on how the smooth background in the spectrum is drawn (Fig. 22). The reason for the discrepancy is not yet clear.

One of the reasons[92] for the discrepancy may be the fact that the radial wave functions of the $J^\pi = 2^+$ level in ^{6}Li and ^{6}He differ. The level is situated in the continuum. In ^{6}Li it is broad, being situated appreciably above the breakup threshold; in ^{6}He it is lower and narrower. It could be that in ^{6}Li a component with isospin $T = 0$ is mixed with the wave function of this level. The corresponding level in ^{6}Li is very broad.

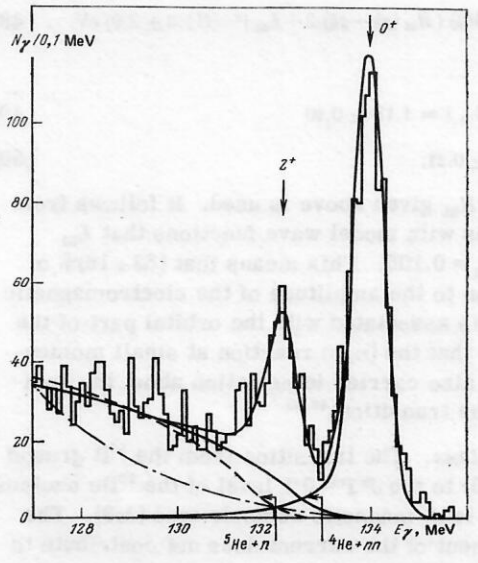

FIG. 22. High-energy part of the γ spectrum for the $^6\text{Li}(\pi,\gamma)^6\text{He}$ raction[22] obtained with resolution improved compared with the data given in Fig. 5. The continuous curve is the result of analysis of the experimental data under the assumption that there are two resonances ($J^\pi = 0^+$ and 2^+) in the excitation spectrum; the broken and chain curves give the contributions of the $^5\text{He}+n$ and $^4\text{He}+2n$ channels in the framework of the pole model.

Analysis of old experimental data on electron scattering in the framework of the cluster model showed that in the $A = 6$ system clusters are not formed to a great degree. Therefore, the shell model encounters difficulties in the interpretation of the experimental electron-scattering data.[99]

The ^{20}Ne *Nucleus.* As follows from the experimental data on inelastic electron scattering in ^{20}Ne, there is a strong $M1$ transition to a level with energy $E^* = 11.24$ MeV.[80 100] It follows from calculations[27] that the main strength of the transition to this level is associated with the orbital part of the current, a situation directly opposite to that in the nucleus ^{6}Li and other nuclei of the $1p$ shell. The weak $M1$ transitions that are manifested in the (π,γ) reaction[23] (see Fig. 15) reflect this feature of the excitation of the ^{20}Ne nucleus.

If we use the phenomenological approach to the (π,γ) reaction described above, we obtain in ^{20}Ne the relation

$$B(\pi^-,\gamma;\ 0^+\to 1^+) = (0{,}9\pm 0{,}5)\,10^{-4} = (6{,}25\pm 2{,}19)10^{-4}\{R_{01}^2 + 0.070\,R_{21}^2 + 0{,}013\,|R_{01}R_{21}^*|\}. \quad (47)$$

Here and below in (52), $B(\pi,\gamma;J_i\to J_f)$ denotes the γ yield. We recall that the integral now contains radial functions of the $1d$ state. The uncertainty in the numerical factor on the right-hand side of (47) is due to the error in the measurement of the width of the $2p$ level in the ^{20}Ne mesic atom.[38] Since the numerical factor in front of the matrix element R_{21} is small, all this term can be ignored, and we then find that $R_{01} = 0.12\pm0.04$. The width of the $J^\pi = 1^+$ level due to $M1$ transition to the ^{20}Ne ground state is related to the matrix elements by[38]

$$\Gamma_{\gamma 0} = (2\pi\alpha/9M_p^2)\,|\,R_{01}\,(g_p^s - g_n^s)/2 + L_{01}\,|^2 = (11.2 \pm 2.0)\ \text{eV}. \quad (48)$$

It follows that

$$|\,L_{01} + 4.7\,R_{01}\,| = 1.17 \pm 0.10 \quad (49)$$

$$L_{01} = 0{,}62 \pm 0.21, \quad (50)$$

if the value of R_{01} given above is used. It follows from the calculations with model wave functions that $L_{01} = 0.605$ and $R_{01} = 0.105$. This means that $(53 \pm 16)\%$ of the contribution to the amplitude of the electromagnetic $M1$ transition is associated with the orbital part of the current. Note that the (n,p) reaction at small momentum transfers also carries information about the spin amplitude of the transition.[42,43]

The ^{10}B Nucleus. The transition from the ^{10}B ground state ($J^\pi T = 3^+0$) to the $J^\pi T = 0^+1$ level of the ^{10}Be nucleus (ground state) is of magnetic octupole type ($M3$). The orbital component of the current does not contribute to the form factor of this transition, and, therefore, it is determined by the unique matrix element R_{23}:

$$F_{M3}(q) = [\sqrt{\pi/(2J_i+1)}\,\sqrt{8/63}/ZM_p r_0] \times y^{3/2}\exp(-y(1+d))\,(g_p^s - g_n^s)\,R_{23}, \quad (51)$$

where $y = (qr_0/2)^2$ and $d = a_p^2/r_0^2 - 1/A$. For radiative pion capture from both the $1s$ and the $2p$ mesoatomic orbits the transition rate is determined solely by the matrix element R_{23}:

$$B(\pi,\ \gamma) = (4{,}91 \pm 0.37)10^{-4} R_{23}^2. \quad (52)$$

The numerical factor in (52) is obtained on the basis of the mesoatomic parameters given in Table VI of Ref. 1: $\omega_{1s} = 1 - \omega_{2p} = 0.20 \pm 0.05$, $C_{1s} = 0.52$, $C_{2p} = 1.38$, $\Gamma_{1s} = 1.68 \pm 0.12$ keV, $\Gamma_{2p} = 0.32 \pm 0.06$ eV. It follows from the electron-scattering data that $R_{23} = 0.70 \pm 0.06$, and from the radiative-pion-capture data that $R_{23} = 0.64 \pm 0.04$, which agrees well with the first value.

The following maximum in the γ spectrum of radiative pion capture by the ^{10}B nucleus corresponds to excitation of a $J^\pi = 2^+$ level. The electromagnetic $J^\pi = 3^+ \to 2^+$ transition is associated with operators of the following multipoles: $M1$, $E2$, and $M3$. In this case, the radiative pion capture is determined by the matrix elements R_{01}, R_{21}, R_{22}, R_{23}, and $R_2 = \langle 2^+ \| Y_2 \tau_- \| 1^+ \rangle$. As follows from the experimental data on electron scattering, the $M1$ transition is manifested only at momentum transfer around 0.7 F^{-1}. The longitudinal component of the current is hardly manifested.

It follows from what we have said that the matrix elements R_{01}, R_{21}, and R_2 can be ignored. At large momentum transfers, it is difficult to distinguish an $E2$ transition from an $M3$, since in the absence of a convection current they both have the same dependence on the momentum transfer. If we assume that we have here a pure $M3$ transition, then $R_{23} = 1.09 \pm 0.06$ on the basis of the electron-scattering data and $R_{23} = 1.05 \pm 0.05$ according to the (π,γ) reaction. The agreement is very good. From this it may be concluded that the contribution of the $E2$ transition is small. This result agrees with the result obtained using model wave functions. In the latter case, there is a contribution of magnetic dipole excitation.

A different picture is observed for transition to the $J^\pi = (2^+1)_2$ level. The $M1$ transition is predominant in the excitation of this level. Simultaneous analysis of the data on the (e,e') and (π,γ) reactions leads to the matrix elements

$$L_{01} = -0{,}8 \pm 0.1; \quad (53a)$$

$$L_{01}/R_{01} = -1.03 \pm 0.20. \quad (53b)$$

These examples have enabled us to illustrate the possibilities of the approach. This method can be used in all cases when besides radiative-pion-capture data there are data on $M1$ transitions, as, for example, in ^{12}C (Refs. 22 and 72), ^{13}C (Ref. 23), ^{14}N (Refs. 22, 48, and 72), ^{28}Si (Ref. 53), ^{32}S (Ref. 84), etc. We refer the reader to the original papers, in which these transitions are analyzed.

The method of phenomenological analysis has undoubted attraction, since it is an attempt to reduce the model dependence of the results. In evaluating particular conclusions, one must, however, use caution. The existence of unresolved structures (for example, overlapping levels of different spins and parities), the extrapolation of form-factor values to other momentum transfers, and other factors may significantly reduce the information content of the approach. The method of phenomenological analysis is not universal and applies only in the cases when there already exists fairly complete experimental information about the given nuclear system.

4. PROSPECTS FOR FURTHER DEVELOPMENT OF INVESTIGATIONS OF RADIATIVE CAPTURE OF PIONS

A review of the state of experimental and theoretical investigations of radiative pion capture would be incomplete without a discussion of possible ways of further development of investigations in this field. Simple extension of the existing method to other nuclei and an increase in the statistics of the observed events would hardly lead to the acquisition of qualitatively new information. It is not difficult to see the new directions in which the investigations must advance. For this, it is sufficient to establish what are the limitations of the existing data and what hinders their detailed theoretical analysis. An obvious shortcoming of the experimental data on radiative pion capture, even if better resolution were achieved, is that we always observe the response of the nucleus for fixed (for given excitation energy) value of the momentum transfer, which is close to the pion rest mass. Using only data on radiative pion capture from a mesoatomic orbit, one cannot determine the spins and parities of the observed resonances. A comparison with results of calculations that is aimed at establishing the quantum numbers of the resonances must be made using data from other related processes in the same nucleus, or one must use theoretical arguments that we wish to test. Further, in a quantitative comparison the inadequacy of the existing information about the properties of mesoatomic levels is clearly revealed.

Direct measurement of the width of the $2p$ level by a crystal-diffraction spectrometer can be done only for nuclei with atomic number $A \gtrsim 16$.[101] Thus, new measurements for nuclei of the $1p$ shell, in which a number of contentious points have arisen, must be matched to model-dependent calculations of the cascade and γ yields. Although one cannot expect a significant improvement in the accuracy of the measurements in this direction, one can attempt to clarify the situation in the nuclei in which there is the most acute contradiction with theory. Generally, the widths of the $1s$ levels are known with greater accuracy[102] (see also Table VI in Ref. 1). Therefore, coincidence measurements like those realized[62] in ^{6}Li can be extended to other nuclei of the $1p$ shell. The decrease in the γ yield from the $2p-1s$ transition will be partly compensated by the increased energy of the x rays. In addition, the intensity of the meson beam has also been increased since 1976, when the ^{6}Li experiments were made.

It is now possible to place some confidence in the optical potentials extracted from pion elastic-scattering data. Therefore, measurements of radiative capture of pions in flight[103] are a natural continuation of the work in this field. In such a case, one can vary the momentum transfer to ensure that the transitions of the multipolarity in which one is interested are dominant, which makes it possible to determine the quantum numbers of the levels directly from the experiment.

Using pion beams of the existing meson factories, one can achieve momentum transfers in the interval from 0.2 to 3 F^{-1}. Figure 23 shows as an example the result[104] of calculating the $^{16}O(\pi^-, \gamma)$ reaction cross section. The pion energy is 60 MeV. The figure reflects the typical behavior of cross sections for levels with different spin values. At this energy of the incident pion, the momentum transfer reaches the value 1.5 F^{-1}.

In emphasizing the advantages of in-flight radiative capture of pions, we must also emphasize that these investigations are very difficult at the practical level.

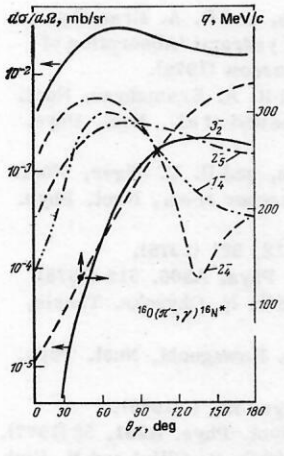

FIG. 23. Angular distribution of photons in the $^{16}O(\pi, \gamma)$ reaction with excitation of different levels of the ^{16}N nucleus; $E_\pi = 60$ MeV.[104] The broken curve (right-hand scale) shows the dependence of the momentum transfer on the angle for $E_\pi = 60$ MeV; the continuous curve corresponds to the total contribution of the negative-parity levels.

TABLE XIII. Typical parameters of facility required for radiative capture of pions in flight in the $^{13}C(\pi^+, \gamma)^{13}N$ reaction at $E_\pi = 120$ MeV.

Momentum spread of beam	±0.65%	1.05*
Thickness of target	0.22 cm	1.05*
Resolution of spectrometer		1.05*
Total resolution (FWHM for $E_\gamma = 250$ MeV), MeV		1.80
Acceptance, $\Delta\Omega\eta_\gamma$		$3 \cdot 10^{-4}$
Particle flux, sec^{-1}		$3 \cdot 10^8$
Number of events, $[\mu b \cdot sr^{-1} \cdot h^{-1}]^{-1}$		4

*Contribution to total resolution, MeV

Therefore, an extensive program of investigations is ruled out. Let us list the limiting factors. To identify the contributions of individual levels, it is necessary to achieve the same resolution as for radiation pion capture from mesoatomic orbits, but now for γ rays of higher energy. The resolution problem is also aggravated here by the circumstance that one must reckon with energy loss of the pions in the target and with a spread of momenta in the beam itself. As an example, Table XIII gives the parameters of a facility necessary for separating the contributions of the ground and first excited state in ^{13}N to the $^{13}C(\pi^+, \gamma)$ reaction. This result was obtained in a methodological experiment made at SIN.[105]

In Table XIII, we also give the expected rate of accumulation of events. This example, and also the earlier results obtained at Los Alamos,[23 106 107] show (Fig. 24) how difficult it is to perform experiments on the in-flight radiative capture of pions despite the fact that the background conditions are rather favorable. Indeed, beyond the kinematic limit of the charge-exchange reaction there is almost no background problem at all, which makes it possible to study the region of excitation energies of the nucleus up to 30 MeV.

It follows from what we have said that such experiments will probably be made in the cases when one can expect an unambiguous answer to specific or interesting questions. As an example, we may mention the $^{13}C(\pi^+,$

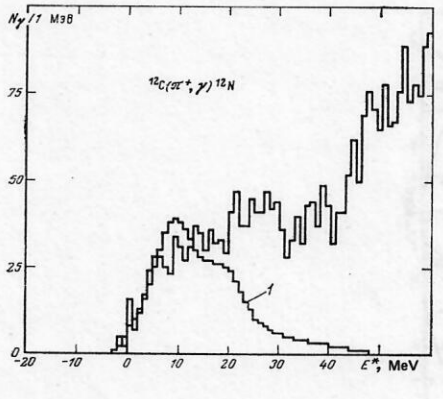

FIG. 24. The γ spectrum for radiative capture of pions in flight[23] in the $^{12}C(\pi^+, \gamma)$ reaction at $E_\pi = 46$ MeV. The background events from the $^{12}C(\pi^+, \pi^0)$ reaction first appear at excitation energy $E^* = 40$ MeV of the nucleus. 1) The result of convolution of the calculated[108] transition-strength distribution with the resolution curve.

γ) reaction, for which an appreciable growth of the differential cross section at angles $\theta > 60°$ is expected if the so-called *critical-opalescence* effect[109] is manifested. Experimentally, a much more favorable situation is created in study of another discussed possibility of direct determination of the spin of a nuclear state. Such a possibility arises if one observes the correlation between the γ ray and any particle produced by the decay of the final nucleus (Refs. 2, 3, 16, 110, and 111). To indicate the characteristic features of such experiments, we discuss in somewhat more detail the $^{16}O(\pi^-, \gamma n)^{15}N$ reaction. The characteristic curves of the angular distributions for levels with different values of the spins obtained in Ref. 16 are given in Fig. 25. The shell model with allowance for the continuous spectrum was used. Figure 25 also gives the dependence of the energies of the neutrons on the angle of their emission to emphasize that measurements based on the time-of-flight method with moderate resolution (for example, 1.5 nsec for a 2-m base) give an energy resolution of order 100 keV if one can simultaneously achieve a resolution of 2° for the emission angle of the photon. In this case, it is not necessary to determine accurately the photon energy. A detector with moderate resolution (for example, a NaI crystal formed from individual cells measuring $6\times6\times40$ cm with 6% resolution at E_γ = 130 MeV, Ref. 112) makes it possible to reduce the number of random coincidences and the influence of other background sources, for example, neutrons. At a pion flux of 10^7 sec^{-1} and using the neutron detector described in Ref. 113 and the NaI crystals in a matrix containing 64 cells, we obtain the following estimate for the rate of accumulation of events: 250 sec^{-1} for the strongest $J^\pi = 2^-$ transition in ^{16}O with small (approximately 10%) background of random coincidences. At the same time, the events can be accumulated simultaneously for six series, an interval of 5° corresponding to each.

This example shows that coincidence experiments are perfectly realistic using the existing technical means. Such experiments will undoubtedly significantly extend our understanding of the mechanism of radiative capture of pions. The results of two such experiments were already published a number of years ago.[114,115] However, the resolution and statistics were unsatisfactory, and these results did not make it possible to draw any definite conclusions.

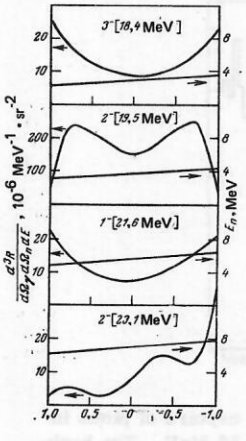

FIG. 25. Angular distribution of neutrons from the decay $^{16}N^* \to {}^{15}N$ (ground state) $+n$ as a result of radiative pion capture by the ^{16}O nucleus.[16] The straight line (to which the right-hand scale corresponds) indicates the neutron energy.

It must be emphasized that the ^{16}O nucleus is a felicitous target, since in the daughter nucleus ^{15}N there is an energy gap between the ground state and the nearest excited state at $E^* = 5.3$ MeV. If there exist several almost degenerate states of the daughter nucleus, one must also attempt to detect the de-excitation γ rays with good resolution. Then the rate of accumulation of events is decreased by about 50 times, i.e., by the factor that determines the conversion efficiency of the pair spectrometer. However, even in this case the experiment can be done in deuterium,[116] as is shown by the example of observation of the (γ, n) correlation.

Of course, the correlation experiments are not restricted to the observation of decay neutrons. One can also detect other particles or photons accompanying the decay of the levels of the daughter nucleus and even the nucleus formed after neutron emission. To analyze the part played by clusters in the spectrum of high excitations of ^6Li one can detect γ rays in coincidence with deuterons or tritium nuclei. In the literature there are several examples of coincidence experiments of this type.

One of the authors (M. Gmitro) would like to thank the administration of the Physics Institute of the University of Zurich for hospitality during his visit, which made it possible, in particular, to complete the work on this review.

[1]M. Gmitro, H. R. Kissener, P. Truöl, and R. A. Éramzhyan, Fiz. Elem. Chastits At. Yadra **13**, 1230 (1982) [Sov. J. Part. Nucl. **13**, 513 (1982)].
[2]H. W. Baer, K. M. Crowe, and P. Truöl, Adv. Nucl. Phys. **9**, 177 (1977).
[3]V. V. Balashov, G. Ya. Korenman, and R. A. Éramzhyan, Pogloshchenie mezonov atomnymi yadrami (Absorption of Mesons by Nuclei), Atomizdat, Moscow (1978).
[4]H. U. Jäger, H. R. Kissener, and R. A. Eramzhyan, Nucl. Phys. **A171**, 16, 584 (1971); A. Aswad *et al.*, Nucl. Phys. **A208**, 61 (1973).
[5]H. R. Kissener, R. A. Éramzhyan, and H. U. Jäger, Nucl. Phys. **A207**, 78 (1973); H. R. Kissener *et al.*, Nucl. Phys. **A219**, 601 (1974).
[6]H. W. Baer *et al.*, Phys. Rev. C **12**, 921 (1975).
[7]N. Ohtsuka and H. Ohtsubo, Nucl. Phys. **A306**, 513 (1978); Prog. Theor. Phys. **64**, 2128 (1980); N. Ohysuka, Thesis, Osaka University (1978).
[8]H. Ohtsubo, T. Nishiyama, and M. Kawaguchi, Nucl. Phys. **A224**, 164 (1974).
[9]S. Cohen and D. Kurath, Nucl. Phys. **73**, 1 (1965).
[10]H. U. Jäger and M. Kirchbach, Nucl. Phys. **A291**, 52 (1977).
[11]V. Gillet, Nucl. Phys. **51**, 410 (1964); V. Gillet and N. Vinh Mau, Nucl. Phys. **54**, 321 (1964); V. Gillet and E. A. Sanderson, Nucl. Phys. **54**, 472 (1964).
[12]D. J. Millener and D. Kurath, Nucl. Phys. **A255**, 315 (1975).
[13]T. T. S. Kuo, Nucl. Phys. **A103**, 71 (1967).
[14]F. C. Barker, Nucl. Phys. **83**, 418 (1966).
[15]L. Rosenfeld, Nuclear Forces, North-Holland, Amsterdam

(1948).
[16]V. V. Balashov and R. Wünsch, J. Phys. G **4**, L239 (1978); R. Wünsch, Nucl. Phys. **A336**, 446 (1980).
[17]R. A. Éramzhyan *et al.*, Nucl. Phys. **A290**, 294 (1977).
[18]H. R. Kissener *et al.*, Nucl. Phys. **A312**, 394 (1978).
[19]H. R. Kissener and R. A. Éramzhyan, Nucl. Phys. **A326**, 289 (1979).
[20]G. Bardin *et al.*, Phys. Lett. **B79**, 52 (1978).
[21]N. C. Mukhopadhyay, Phys. Rep. **C30**, 1 (1977).
[22]A. Perrenoud *et al.*, Report, University of Lausanne (1981).
[23]C. J. Martoff, Thesis, University of California, Berkeley (1980).
[24]H. R. Kissener *et al.*, Nucl. Phys. **A302**, 523 (1978).
[25]H. R. Kissener *et al.*, Report Zfk, Rossendorf (1979).
[26]B. H. Wildenthal *et al.*, Phys. Rev. C **4**, 1708 (1971).
[27]B. H. Wildenthal and W. Chung, in: Mesons in Nuclei (eds. M. Rho and D. H. Wilkinson), Vol. II, North-Holland, Amsterdam (1979), p. 721.
[28]J. P. Perroud, Invited Talk, in: Fifth Seminar on Electromagnetic Interactions of Nuclei at Low and Intermediate Energies, Nauka, Moscow (1981), p. 26.
[29]L. W. Fagg, Rev. Mod. Phys. **47**, 683 (1975).
[30]J. B. Flanz *et al.*, Phys. Rev. Lett. **43**, 1922 (1979).
[31]A. Yamaguchi *et al.*, Phys. Rev. C **3**, 1750 (1971).
[32]A. Richter, Invited Talk, in: Intern. Conf. on Nuclear Physics with Electromagnetic Interactions (eds. H. Arenhövel and D. Drechsel), Mainz (1979), p. 19; A. Richter and W. Knüpfer, in: Intern. School of Intermediate Energy Nuclear Physics, Ariccia, Rome (1979).
[33]H. Davies, H. Muirhead, and J. N. Woulds, Nucl. Phys. **78**, Nucl. Phys. **78**, 673 (1966).
[34]G. Bertsch, Nucl. Phys. **A354**, 157 (1981).
[35]Ch. D. Goodman, Invited Talk, Ninth ICOHEPANS, Versailles (1981); A. Richter, Introductory Report at Session B, Ninth ICOHEPANS, Versailles (1981).
[36]W. Steffen *et al.*, Phys. Lett. **B95**, 23 (1980).
[37]L. L. Foldy and J. D. Walecka, Phys. Rev. **140**, B1339 (1965).
[38]C. J. Martoff *et al.*, Phys. Rev. Lett. **46**, 891 (1981).
[39]F. Ajzenberg-Selove and T. Lauritsen, Nucl. Phys. **A227**, 1 (1974); F. Ajzenberg-Selove, Nucl. Phys. **A248**, 1 (1976); **A268**, 1 (1976).
[40]J. C. Alder *et al.*, in: Proc. of the Intern. Topical Conf. on Meson Nuclear Physics, Pittsburgh (1976).
[41]J. C. Alder *et al.*, in: Photopion Nuclear Physics (ed. P. Stoker), Plenum Press, New York (1979), p. 101.
[42]F. P. Brady and G. A. Needham, in: The (n,p)-Reaction and the Nucleon–Nucleon Force (eds. Ch. D. Goodman *et al.*), Plenum Press (1980), p. 357.
[43]Ch. D. Goodman *et al.*, Phys. Rev. Lett. **44**, 1755 (1980).
[44]A. N. Boyarkina, Izv. Akad. Nauk SSSR, Ser. Fiz. **28**, 337 (1964).
[45]B. Goulard *et al.*, Phys. Rev. C **16**, 1999 (1977).
[46]A. Figureau and N. C. Mukhopadhyay, Nucl. Phys. **A338**, 514 (1980).
[47]H. G. Clerc and E. Kuphal, Z. Phys. **211**, 451 (1968).
[48]A. Perrenoud, Thesis, University of Lausanne (1980).
[49]E. Belloti *et al.*, SIN Physics Report No. I (1976), p. 41.
[50]M. Giffon *et al.*, Phys. Rev. C **24**, 241 (1981).
[51]A. P. Bukhvostov *et al.*, Acta Phys. Pol. **B3**, 375 (1972); H. R. Kissener *et al.*, Nucl. Phys. **A215**, 424 (1973).
[52]E. J. Ansaldo *et al.*, Nucl. Phys. **A322**, 237 (1979).
[53]J. P. Perroud, in: Photopion Nuclear Physics (ed. P. Stoler), Plenum Press, New York (1979), p. 69.
[54]N. C. Mukhopadhyay, Phys. Lett. **B44**, 33 (1973); **B45**, 309 (1973).
[55]J. C. Bergström *et al.*, Phys. Rev. C **4**, 1514 (1971).
[56]Y. R. Calarco *et al.*, in: Workshop on Nuclear Structure with Medium Energy Probes, LASL (1980).
[57]W. Knüpfer, M. Dillig, and A. Richter, Phys. Lett. **B95**, 349 (1980).
[58]B. Mottelson, in: Elementary Modes of Excitation (eds. A. Bohr and R. A. Broglia), North-Holland, Amsterdam (1977).
[59]B. S. Ishkhanov *et al.*, Fiz. Elem. Chastits At. Yadra **12**, 905 (1981) [Sov. J. Part. Nucl. **12**, 362 (1981)].
[60]G. E. Dogotar *et al.*, J. Phys. G **5**, L221 (1979).
[61]R. A. Éramzhyan, M. Gmitro, and H. R. Kissener, Nucl. Phys. **A338**, 436 (1980).
[62]D. Renker *et al.*, Phys Rev. Lett. **41**, 1279 (1978).
[63]R. A. Sakaev and R. A. Éramzhyan, Soobshcheniya (Communication) R2-9610 [in Russian], JINR, Dubna (1976).
[64]J. Bistirlich *et al.*, Phys. Rev. Lett. **25**, 960 (1970).
[65]P. Truöl *et al.*, Phys. Rev. Lett. **32**, 1268 (1974).
[66]J. P. Miller *et al.*, Nucl. Phys. **A343**, 347 (1980).
[67]B. Gabioud *et al.*, Phys. Rev. Lett. **42**, 1508 (1979).
[68]A. S. Cherkasov, Yad. Fiz. **28**, 639 (1978) [Sov. J. Nucl. Phys. **28**, 328 (1878)].
[69]Y. Horikawa, F. Lenz, and N. C. Mukhopadhyay, Phys. Rev. C **22**, 1680 (1980).
[70]J. Ahrens *et al.*, Nucl. Phys. **A251**, 479 (1975).
[71]H. W. Baer *et al.*, in: Ninth ICOHEPANS, Versailles (1981), Contr. H52, p. 339.
[72]H. R. Kissener and R. A. Eramzhyan, in: Photopion Nuclear Physics (ed. P. Stoler), Plenum Press, New York (1979), p. 117.
[73]G. E. Dogotar *et al.*, Report E2-11296 [in English], JINR, Dubna (1978).
[74]B. H. Patrick *et al.*, J. Phys. G **1**, 874 (1975); J. W. Jury *et al.*, Phys. Rev. C **19**, 1684 (1979).
[75]F. Y. Kline *et al.*, Nuovo Cimento **A23**, 137 (1974).
[76]N. Ensslin *et al.*, Phys. Rev. C **19**, 569 (1979).
[77]G. Strassner *et al* ., Phys. Rev. C **20**, 248 (1979).
[78]J. P. Elliott and B. H. Flowers, Proc. R. Soc. London Ser. A **229**, 536 (1955).
[79]G. Hock, Report R4-6102 [in Russian], JINR, Dubna (1971).
[80]W. L. Bendel *et al.*, Phys. Rev. C **3**, 1821 (1971).
[81]W. Knüpfer *et al.*, Phys. Lett. **B66**, 305 (1977).
[82]R. Schneider *et al.*, Nucl. Phys. **A323**, 13 (1979).
[83]B. H. Wildenthal *et al.*, Phys. Lett. **B26**, 692 (1968).
[84]J. E. Alder *et al.*, in: Photopion Nuclear Physics (ed. P. Stoler), Plenum Press, New York (1979), p. 107; P. Truöl, in: Proc. of the Intern. Conf. on Nuclear Physics with Electromagnetic Interactions, Mainz (1979); Lecture Notes in Physics, Vol. 108, p. 351.
[85]R. A. Eramzhyan *et al.*, Czech. J. Phys. **B28**, 1080 (1978).
[86]J. C. Alder *et al.*, in: Seventh ICOHEPANS, Zürich (1977), Contr. **C15**, p. 44.
[87]K. Ebert and J. Mayer-ter-Vehn, Phys. Lett. **B77**, 24 (1978).
[88]C. W. Kim and H. Primakoff, Phys. Rev. **140**, B566 (1965).
[89]W. Maguire and C. Werntz, Nucl. Phys. **A205**, 211 (1973).
[90]P. Szydlik and C. Werntz, Phys. Lett. **B51**, 209 (1974).
[91]J. C. Bergström, I. P. Auer, and R. S. Hicks, Nucl. Phys. **A251**, 401 (1975).
[92]J. C. Bergström, Phys. Rev. C **21**, 2496 (1980).
[93]R. S. Willey, Nucl. Phys. **40**, 529 (1963).
[94]J. B. Cammarata and T. W. Donnelly, Nucl. Phys. **A267**, 365 (1976).
[95]R. Neuhausen and R. M. Hutcheon, Nucl. Phys. **A164**, 497 (1970).
[96]J. Deutsch *et al.*, Phys. Lett. **B26**, 315 (1968).
[97]G. Audit *et al.*, Phys. Rev. C **15**, 1415 (1979).
[98]L. Majling *et al.*, Report No. 205, Lebedev Institute of Physics, Moscow (1980).
[99]Yu. A. Kudeyarov *et al.*, Yad. Fiz. **4**, 1048 (1966) [Sov. J. Nucl. Phys. **4**, 751 (1967)]; Yu. A. Kudeyarov and R. A. Éramzhyan, Yad. Fiz. **9**, 494 (1969) [Sov. J. Nucl. Phys. **9**, 283 (1969)].
[100]F. Aizenberg-Selove, Nucl. Phys. **A300**, 1 (1978).
[101]H. Leisi, ETH Zürich Report (1981).
[102]G. Backenstoss, Ann. Rev. Nucl. Sci. **20**, 467 (1970).

[103]G. W. Reynaud and F. Tabakin, Phys. Rev. C 23, 2652 (1981).
[104]M. Gmitro *et al.*, Sbornik annotatsiĭ (Collection of Annotations), Khar'kov (1982).
[105]C. J. Martoff *et al.*, SIN Proposal R80-08.
[106]P. Truöl, Nucl. Phys. A335, 55 (1980).
[107]J. P. Miller *et al.*, Bull. Am. Phys. Soc. 24, 647 (1979).
[108]F. Cannata *et al.*, Can. J. Phys. 52, 1405 (1974).
[109]J. Delorme, in: Workshop "From Collective States to Quarks in Nuclei," Bologna (1980); Report LYCEN 8088, October (1980); K. M. Crowe *et al.*, in: Ninth ICOHEPANS, Versailles (1981), Contr. J20, p. 405.
[110]R. A. Eramzhyan, M. Gmitro, and L. A. Tosunjan, J. Phys. G 4, L233 (1978); Czech. J. Phys. B29, 370 (1979).
[111]V. V. Balashov *et al.*, Fiz. Elem. Chastits At. Yadra 4, 585 (1973) [Sov. J. Part. Nucl. 4, 247 (1973)].
[112]A. Bay *et al.*, SIN Newsletter 14, NL65 (1982).
[113]M. T. Tran *et al.*, Nucl. Phys. A324, 301 (1979).
[114]W. C. Lam *et al.*, Phys. Rev. C 10, 72 (1974).
[115]J. C. Alder *et al.*, Lett. Nuovo Cimento 4, 256 (1970).
[116]B. Gabioud, Thesis, University of Lausanne (1980).

Translated by Julian B. Barbour